Journal of Asian Earth Sciences: X 2 (2019) 100010

Contents lists available at ScienceDirect

Journal of Asian Earth Sciences: X

journal homepage: www.journals.elsevier.com/journal-of-asian-earth-sciences-x

Diverse depositional and geochemical signatures of the Frasnian-Famennian global event in western Thailand reveal palaeotethyan vs. Western Australian geotectonic affinities

Grzegorz Racki[a,*], Peter Königshof[b], Zdzislaw Belka[c], Jolanta Dopieralska[d], Agnieszka Pisarzowska[a,e]

[a] Department of Earth Sciences, Silesian University in Katowice, Sosnowiec, Poland
[b] Senckenberg Research Institute and Natural History Museum, Frankfurt, Germany
[c] Adam Mickiewicz University, Isotope Laboratory, Poznań, Poland
[d] Poznan Science and Technology Park, Adam Mickiewicz University Foundation, Poznań, Poland
[e] Institute of Geological Sciences, Polish Academy of Sciences – Research Centre in Cracow, Cracow, Poland

ARTICLE INFO

Keywords:
Frasnian-Famennian biocrisis
Thailand
Geochemistry
Biostratigraphy
Paleogeography

ABSTRACT

Two studied sections of the Frasnian-Famennian (F-F) boundary beds in western Thailand differ significantly in their depositional and geochemical characteristics. The highly condensed, monotonous Mae Sariang (MS) limestone succession generally corresponds to the event-chemostratigraphic pattern of the F-F biocrisis based primarily on German sections, and brief anoxic episodes are identifiable in trace-metal signatures (but neither organic-rich intercalations nor distinct volcanic signals). In the case of the Thong Pha Phum (TPP) site, two specific features are especially notable: (1) a $\delta^{13}C$ positive excursion, comparable only with the peculiar Western Australian biogeochemical signature, and (2) elemental proxies that indicate exclusively oxic and probably largely oligotrophic conditions during both Kellwasser intervals. Therefore, the demonstrated biogeochemical and environmental differentiation confirms the totally different paleogeographic settings of the studied successions, as indicated previously by the Nd isotope composition of Late Devonian seawater. The distinctiveness of the TPP section clearly indicates its affinity with the Western Australian shelf successions, which are characterized by a well-known "atypical" biogeochemical and ecological signature. In terms of provenance, the siliciclastic fraction in the MS succession corresponds to continental margin. The Paleotethyan region was sourced by felsic-volcanic or granite-gneissic massifs. In the case of the TPP section, the continental margin, as well as the partly the continental island arc, are recorded in the detritus, predominantly derived from older, continental sedimentary-metasedimentary terrains. Therefore, the assumed Western Australian geotectonic assignment of TPP corresponds to the variable, partly recycled material supplied abundantly to the "Sibumasu depocenter" from adjoining granite-dominated Archean cratons.

1. Introduction

Strongly folded and thrusted Upper Devonian strata are reported from a number of regions in Thailand (e.g., Savage et al., 2006; Fontaine et al., 2009; Thassanapak et al., 2017). As a result of limited stratigraphic work, their timing and the relationships of their facies remain mostly vague. These correlations and basin reconstructions are additionally obscured by the conjectural relationships of the Southeast Asian continental crust, terrane/continental blocks, volcanic arcs, and suture zones of lost oceanic basins accreted recently in the Indochina Peninsula (e.g., Dopieralska et al., 2012; Wang et al., 2018). On the other hand, the current advancement is clearly exemplified by chert-carbonate and volcanic sequences of the Indochina terrane in north-eastern Thailand (and adjacent regions of Laos), for which biostratigraphical, facies, and geochemical data have been provided (Thassanapak et al., 2017; Udchachon et al., 2017a, 2017b; see also Hara et al., 2010).

In the western part of Thailand, the Upper Devonian is represented mainly by pelagic or hemipelagic limestone successions. Thanks to the work of Norman Savage's research group, two sections have been reliably dated by means of conodont faunas and combined with geochemical and microfacies/sedimentology data, including the key

* Corresponding author at: Department of Earth Sciences, Silesian University, Sosnowiec, Poland.
E-mail address: racki@us.edu.pl (G. Racki).

https://doi.org/10.1016/j.jaesx.2019.100010
Received 24 October 2018; Received in revised form 30 July 2019; Accepted 31 July 2019
Available online 21 September 2019

carbon isotope chemostratigraphic signature (Savage et al., 2006; Dopieralska et al., 2012; Königshof et al., 2012; Savage, 2013). This high-resolution bio- and chemostratigraphical framework enables the study of elemental inorganic geochemical signatures across the Frasnian-Famennian (F-F) boundary. Importantly, the localities near the small towns of Thong Pha Phum (TPP) and Mae Sariang (MS) represent two different paleogeographic domains, as evidenced by the neodymium (Nd) isotope composition of seawater reconstructed by Dopieralska et al. (2012). While the more condensed MS succession corresponds to a pelagic realm within the Paleotethys Ocean of the Inthanon Zone, the TPP locality belongs to the outer Australian shelf of northeastern Gondwana (i.e., the Sibumasu terrane; cf. also Torsvik and Cocks, 2017). Therefore, the interpreted F-F environmental changes can be comparatively analyzed in the context of a well-defined geotectonic setting.

The Frasnian-Famennian boundary beds are characterized overall by the co-occurrence of two particular dark, organic-rich shaly Kellwasser (KW) levels. The Upper KW marks a global biotic event corresponding to a major ecosystem perturbation at the F-F boundary, as the dramatic finale of the stepwise KW Crisis (Walliser, 1996; Becker et al., 2012; Gereke and Schindler, 2012; Ma et al., 2016; Huang et al., 2018a; Carmichael et al., 2019; Fig. 1). Recently, this biotic crisis and the resulting disruption of the epeiric carbonate factory (in particular the total collapse of metazoan reefs) have been considered as representing a mass depletion of marine diversity resulting mainly from a reduced origination rate (see Racki, 2005; McGhee, 2013; Stanley, 2016). Remarkably, both Thai sections lack diagnostic black KW-type lithology (time-specific facies *sensu* Walliser, 1984; Gereke and Schindler, 2012; see also data from Vietnam in Komatsu et al., 2019; Königshof et al., 2017), but the occurrence of both KW intervals are indicated by positive carbon isotope excursions (Savage et al., 2006; Königshof et al., 2012; Savage, 2013). As shown in this study, a surprisingly variable record of previously acknowledged global environmental changes characterizes the Thai successions. Not only is this relative uniqueness relevant to understanding the KW Crisis on regional and supra-regional Asiatic-Australian scales, but it also has several implications for the global scenario.

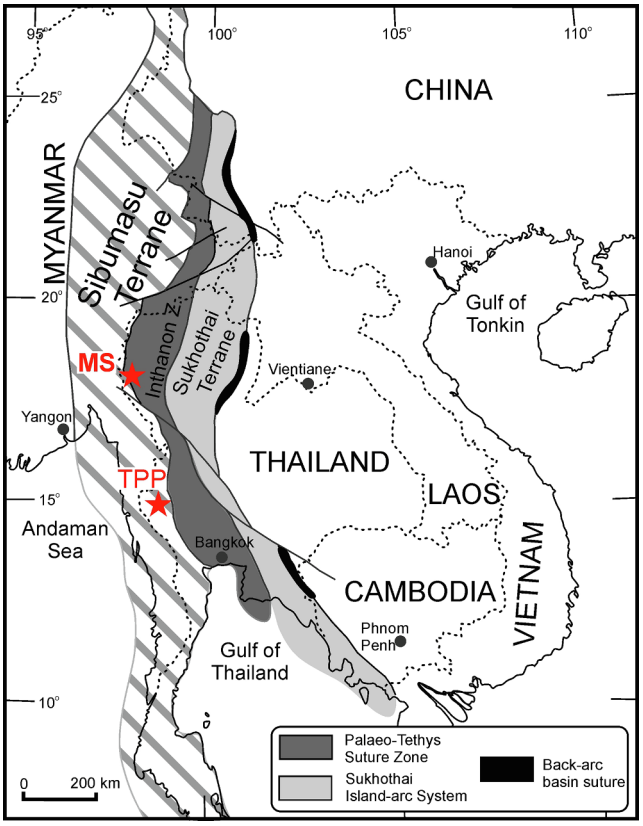

Fig. 2. Tectonic subdivision in Thailand and Southeast Asia (after Sone and Metcalfe, 2008, slightly modified) and location of the studied sections: the MS (Mae Sariang) section is attached to the westernmost part of the Inthanon Zone; the TPP (Thong Pha Phum) section is part of the Sibumasu Terrane.

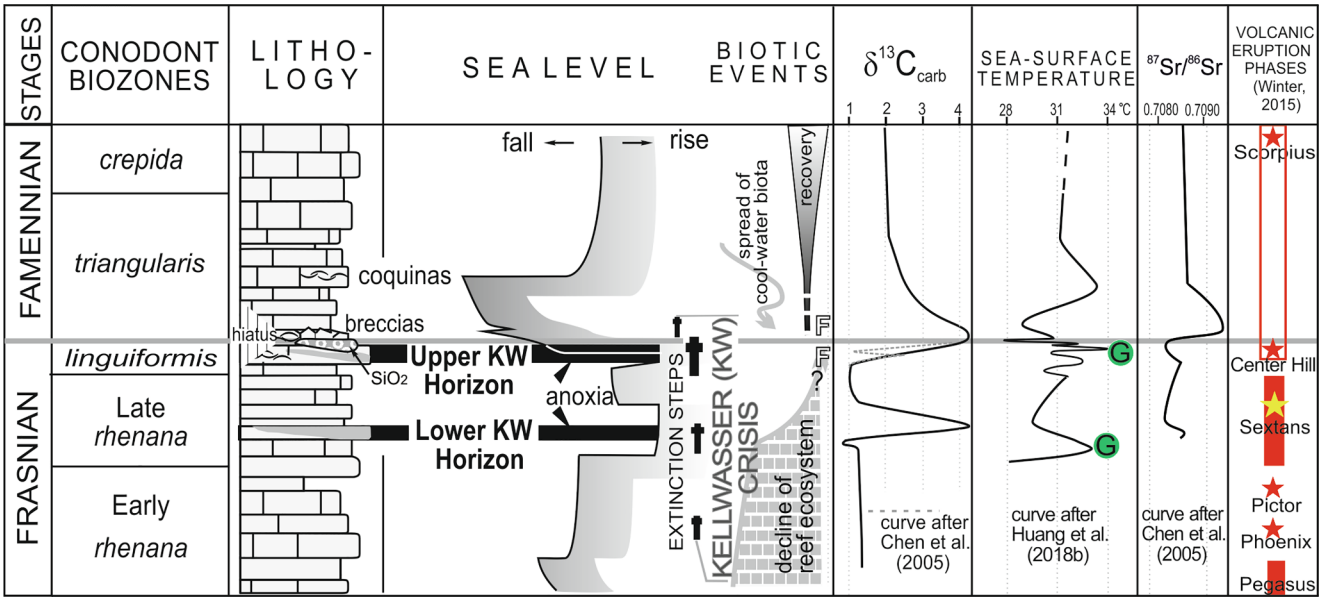

Fig. 1. Diagram showing composite sedimentary and geochemical records across the Frasnian-Famennian transition, and major eustatic, biotic, and volcanic events (compiled from Fig. 2 in Joachimski and Buggisch, 2002, Fig. 2 in Chen et al. 2005, Fig. 1 in Racki et al., 2018b, and Fig. 7 in Huang et al., 2018a; cf. Morrow and Sandberg, 2008, Fig. 2; Gereke and Schindler, 2012, Figs. 1, 9; Ma et al., 2016, Fig. 11; Huang et al., 2018a, Fig. 2). Two greenhouse spikes (G in green) implied from Retallack and Huang (2011). For updated Famennian conodont zonation see Spalletta et al. (2017) and Savage (2019).

1.1. Material and methods

Both Thai limestone sections were progressively sampled by Norman Savage's research group between 2003/04 (TPP) and 2006/07 (MS) and initially processed for conodont faunas only. In 2010 (MS) and 2012 (TPP) the sections were revisited for sedimentological/facies studies. Note that, in fact, the MS section includes the tectonically repeated Upper Devonian strata from the late Frasnian to the D-C transition (Königshof et al., 2012, Fig. 4; Savage, 2013), and only the basal interval of the succession (Late *rhenana* to *crepida* zones; beds MS-D18 to MS-D16) is the subject of geochemical studies in the present paper. Subsequently, both sections were analyzed for carbon and oxygen stable isotope ratios, and the only meaningful results for carbon isotopes were presented in Savage et al. (2006) for TPP and in Königshof et al. (2012) and Savage (2013) for MS.

Nd and Sm isotope data for TPP were collected at the Isotope Laboratory of the Adam Mickiewicz University at Poznań (Poland) on spiked conodont samples using a Finnigan MAT 261 multicollector thermal ionization mass spectrometer. Rare-earth element separation was achieved in accordance with a procedure described by Dopieralska (2003) and Dopieralska et al. (2012).

Abundances of major, minor, and trace elements were determined in 2009 in 33 rock pulp samples (20 from TPP and 13 from MS; provided in 2007 by Norman Savage for Grzegorz Racki), at Acme Analytical Laboratories Ltd., Canada (Vancouver). In addition, a similar set of geochemical data for 7 repeated samples from the lowest bed, MS-D18, was kindly provided by Norman Savage in 2011, but the results are only partially comparable (see Figs. 12 and 17, and Appendix 2). This differentiation likely resulted from difficulties in resampling the condensed carbonate succession in 2010 (Fig. 5B; Savage, 2019); thus the repeated data are used herein to a limited degree (with the exception of the obviously supplementary samples D18-A/2011 and D18-Aex/2011), mostly for the calculation of average contents (Table 1, see Fig. 11) and correlation of elements (Appendix 1). Moreover, Savage (2013) presented elemental geochemical results in the form of plots for the entire MS succession, based on 80 samples measured for him at the same Canadian laboratory, but without detailed discussion of the geochemical proxies and their environmental interpretation across the KW interval.

Total concentrations of the major oxides and several minor elements were reported from a 0.2-g sample analyzed by means of ICP-emission spectrometry following lithium metaborate/tetraborate fusion and dilute nitric digestion. Rare-earth and refractory elements (e.g., Ba, Co, Sr, Th, U, V, Zr) were determined using ICP mass spectrometry following the same decomposition method. A separate 0.5-g split was digested with 3 ml of 2:2:2 HCl–HNO_3–H_2O as well as analyzed using ICP MS for precious and base metals (e.g., Mo, Cu, Pb, Zn, Ni, As, Sb). Total carbon (TC) and total inorganic carbon (TIC) were determined for 2007 samples using an Eltra CS-500 IR-analyzer with a TIC module. TS and TC were determined using an infrared cell detector. TIC content was determined by infrared detector as carbon dioxide derived from carbonates reacted with 15% warm hydrochloric acid. total organic content (TOC) was calculated as the difference between TC and TIC. Instrument calibration utilised the Eltra standards. Analysis were performed in Faculty of Earth Sciences, University of Silesia (Poland). In addition, total carbon and sulfur analyses were supplied by Leco determinator. The reliability of the data was checked via analyses of international standard reference materials. The precision and accuracy of the results were better than ± 0.9% (mostly ± 0.4%) for the 11 major elements and better than ± 15% for the 45 trace elements, considered only in part in this study. Twenty samples were additionally measured for mercury using the refined analytical technique of atomic absorption spectrometry (AAS; detection limit = 0.2 ppb, as compared to10 ppb in ICP MS) at the Faculty of Earth Sciences, University of Silesia (Poland; for discussion of Hg-related analytical issues, see Racki et al., 2018a). When the concentrations of trace metals (especially Mo, Hg, and Cr) were below the detection limits (see Appendix 2), three-fourths of the value below the suitable detection limit value (cf. Racki et al., 2018a) was used; this applies as well to environmental proxy calculations (see Figs. 12, 13, 15, 16 and 19). Spearman rank-order correlation was used to calculate the matrix for the geochemical data (Appendix 1).

Microfacies analysis for MS and TPP was based on more than 147 thin sections. Samples were taken at intervals of several centimeters or less when necessary. The thin sections are stored at the Senckenberg

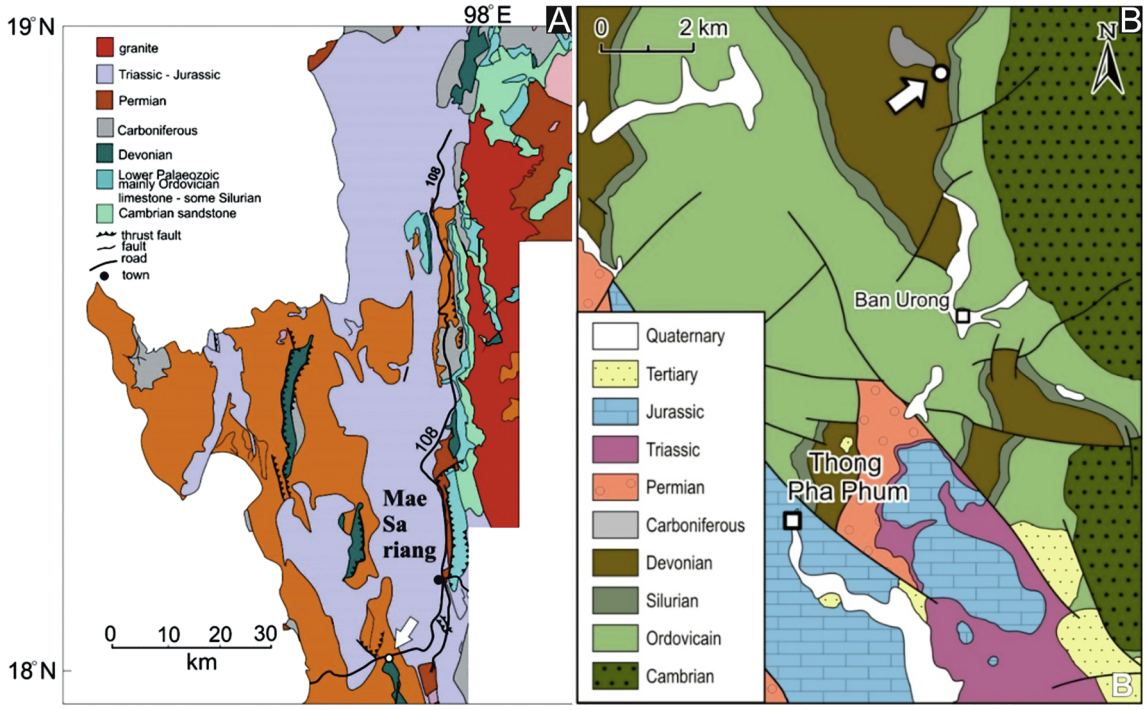

Fig. 3. A: Geological map of the Mae Sariang area (after Baum et al., 1982) with the location of the studied section (arrow). The geology of Myanmar is omitted. B: Geological map of the Thong Pha Phum area (modified from Hagen and Kemper, 1976; after Dopieralska et al., 2012) with the location of the studied section (arrow).

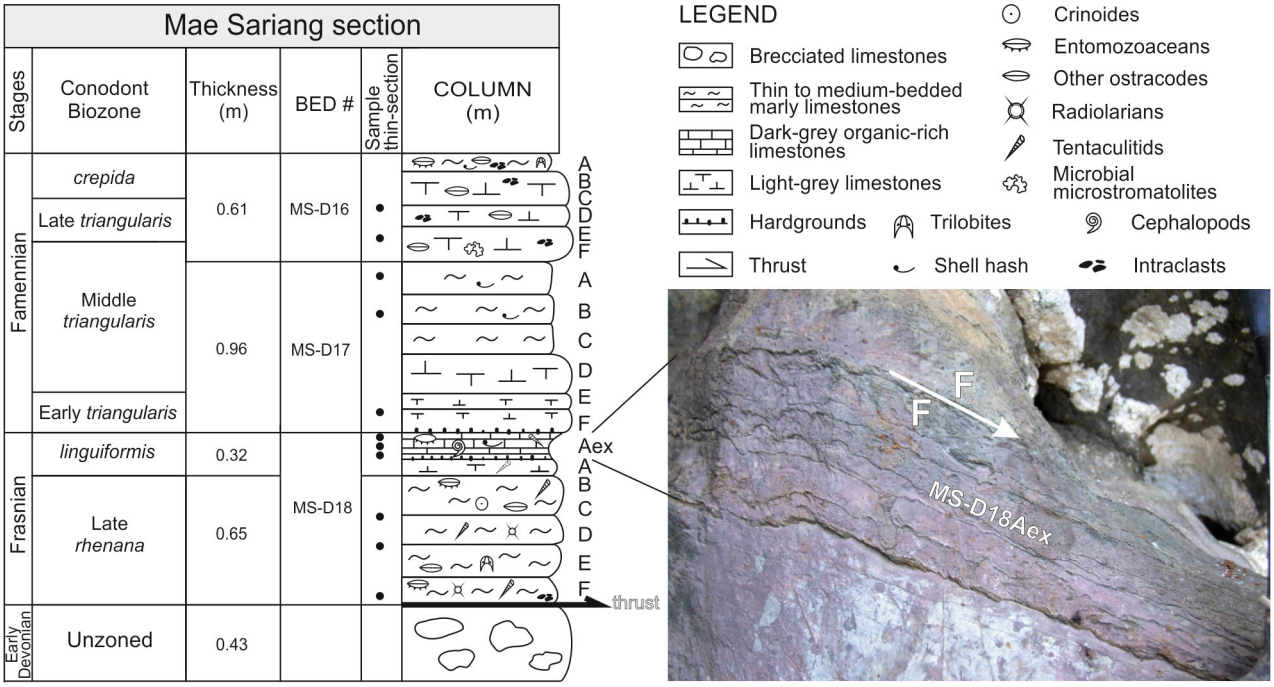

Fig. 4. Lithological and paleontological characteristics of the Mae Sariang section (lower part), and close-up of the key F-F boundary interval. Note the topmost Frasnian layer, marked by the condensed brownish/grayish level D18-Aex (see Fig. 5B, 12; compare Königshof et al., 2012, Fig. 5).

Research Institute and Natural History Museum, Frankfurt am Main, Germany (SMF numbers MS 70509–70589, TPP 70623–70690). Conodont elements are stored at the University of Oregon (materials of Savage et al., 2006; Savage, 2013).

2. Regional geologic setting (Königshof)

Southeast Asia is composed of a number of continental blocks, volcanic arcs, and suture zones. Thailand in particular is characterized by several terranes which originally formed part of Gondwana. During the Paleozoic, these blocks became separated from the northern margin of Gondwana and later became amalgamated with the southern margin of Asia (e.g., Burrett, 1974; Nie et al., 1990; Metcalfe, 1996, 2006, 2011; Sone and Metcalfe, 2008; Ridd, 2009, 2011). The tectonic framework of Thailand can be subdivided into four geotectonic units (Fig. 2): the Sibumasu Terrane (Metcalfe, 1984) in the west, the

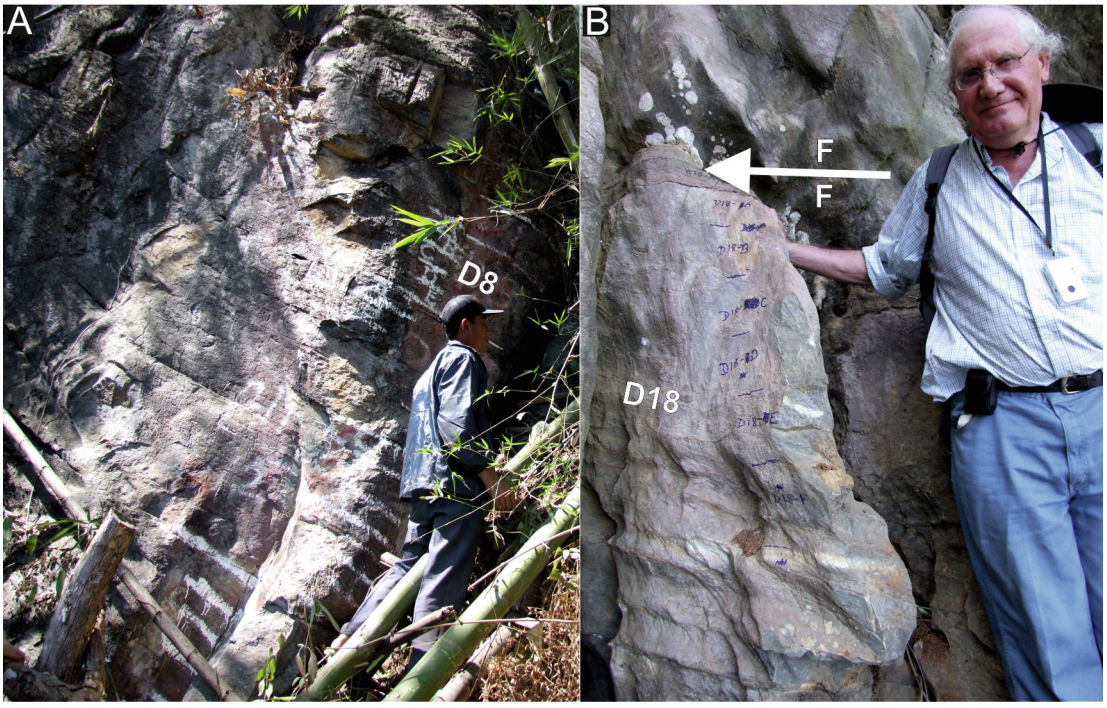

Fig. 5. Field photo of the Mae Sariang locality (A; middle part of the Famennian section; bed D8 – see Königshof et al., 2012, Fig, 4A); and showing the subdivided bed D18 with markings of where samples were taken in 2010 (B; compare Fig. 2 in Savage, 2019), marked by the condensed horizon D18-Aex (Fig. 4) forming the top horizon of the Frasnian succession (arrow).

Inthanon Zone, the Sukhothai Zone, and the Indochina Terrane in the easternmost part of the country (Sone and Metcalfe, 2008). The Sibumasu Terrane covers the western part of northern Thailand, extending westward and northwards into Myanmar and Yunnan and southwards to western Peninsular Malaysia and Sumatra. It is widely accepted that Sibumasu rifted from Gondwana in the Late Carboniferous or later, in the Early Permian, and collided with the Sukhothai/Indochina Terrane in the Middle or Late Triassic (e.g., Sone and Metcalfe, 2008; Ueno and Charoentitirat, 2011; Ridd, 2015). Radiolarian fauna and sedimentological and geochemical data suggest the presence of an ocean between the Sibumasu and other continental terranes in Southeast Asia (Wonganan and Caridroit, 2005; Randon et al., 2006; Wonganan et al., 2007; Hara et al., 2010).

To the east, the Sibumasu Terrane is bounded by the Inthanon Zone (Barr and Macdonald, 1991), which represents an accretionary complex of the Paleotethys Ocean, closed in the Triassic (Metcalfe, 2013). According to Kamata et al. (2009) and Ridd (2015), the Mae Yuam Fault zone marks the boundary between Sibumasu and the Inthanon Zone, whereas the entire Mae Sariang area is assigned to the Inthanon Zone by Metcalfe (2006, 2009). Characteristic rocks of the Inthanon Zone include deep-water radiolarian cherts and Carboniferous-to-Permian carbonates deposited on seamounts (Ueno et al., 2010), as well as black shales, tuffs, and tuffaceous cherts (Hara et al., 2010).

Further to the east is the next tectonic unit, the Sukhothai Terrane (Fig. 2), regarded as a magmatic island arc which developed along the margin of the Khorat Terrane (Sone and Metcalfe, 2008). Finally, the eastern part of Thailand, including the Khorat Plateau, is occupied by the Indochina Terrane, representing a continental block with a Precambrian basement covered by Paleozoic to Mesozoic rocks, and also a part of Gondwana (Metcalfe, 1999; Barber et al., 2011; Ridd, 2012). Paleozoic rocks consist mainly of shallow marine deposits, whereas Mesozoic rocks are of continental origin (Metcalfe, 2006; Morley et al., 2011).

3. Analytical sections and conodont stratigraphy (Königshof)

3.1. Mae Sariang

The Mae Sariang section (Fig. 3A), located southwest of Chiang Mai, is interpreted as belonging to the Inthanon Zone on the basis of sedimentological/facies characteristics described from this section (Königshof et al., 2012). The section was exposed in an almost vertical cliff approximately 20 m thick (following a landslide in 2012, only the lowermost part of the section is accessible), of which 11.6 m comprises Upper Devonian limestones without macrofossils (Figs. 4 and 5). The section, composed of middle- to thick-bedded, light to dark gray limestones (in some layers, clay- or organic-enriched; Fig. 4), ranges from the Late *rhenana* to the *praesulcata* conodont Zones (Savage, 2013) and includes a thrust fault, resulting in the repetition of intervals from the Early to the upper Early *triangularis* Zones (Savage, 2013). Thus we have limited the present study to the basal interval of the section (beds MS-D18 to MS-D16, Fig. 4). The mainly cosmopolitan conodont fauna exhibits some affinities with, along with some differences from, coeval faunas from South China (Savage, 2013, 2019).

3.2. Thong Pha Phum

This section is located near Thong Pha Phum, approximately 350 km south of the Mae Sariang section (Fig. 3B). While the latter represents Upper Devonian rocks from the Inthanon Zone, the former belongs, in structural terms, to the Sibumasu Terrane. The TPP section is mainly composed of thin-bedded reddish and gray nonfossiliferous limestones, marly limestones, and calcareous siltstones in distinct layers, distinctly thicker in the Famennian interval (Fig. 6).

The section is approximately 6.6 m thick and ranges from the Late *rhenana* to the Late *triangularis* conodont Zones, but the lower boundary of the *linguiformis* Zone has not been identified with certainty (Savage et al., 2006). The conodont species described from this section are mainly cosmopolitan, but regional disappearance or extinction has been established at the F-F boundary, along with recovery and the appearance of new species in the Famennian (Savage et al., 2006).

4. Microfacies and depositional environments (Königshof)

Both sections lack typical lithological characteristics such as black organic-rich shales at the F-F boundary (KW horizons, Fig. 1). Generally, both sections exhibit condensed carbonate strata with low sedimentation rates. Some separations between single layers represent hardgrounds and minor breaks in sedimentation. Minor facies differences occur in the MS sections; the sediments of the TPP succession are more diverse.

4.1. Mae Sariang

The limestone strata around the F-F boundary in the MS section are characterized by poor pelagic faunal content. The fauna is dominated by (in ascending order) conodonts, pelagic ostracodes, trilobites, tentaculitids, radiolarians, goniatites, and rare crinoids (Königshof et al., 2012; Fig. 4). The abundance of conodont elements varies from about 20 per kg to several hundreds or even thousands in particular layers, such as in interval MS-D18A, immediately below the F-F boundary (Savage, 2019). A notable feature here is a successional shift from abundant diverse Frasnian faunas, dominated by polygnathids, to palmatolepid-polygnathid biofacies just below the F-F boundary, and finally to impoverished palmatolepid biofacies in the lowermost Famennian (Savage, 2019).

In terms of quantitative microfacies analysis (grain size, fabric), rocks of the MS section are characterized by a monotonous composition of pelagic limestones (MF 1, microbioclastic lime mudstone to wackestone, Fig. 7A). Neither bioturbation nor lamination occurs. Close to the F-F boundary, within the *linguiformis* Zone, the lithology as well as the fossil content differs. Sample MS-D18Aex, 15 cm thick, is equivalent to the UKW Horizon (see Fig. 1) and can be subdivided into four single layers separated by hardgrounds (Königshof et al., 2012, Fig. 6C). The condensed succession (the “brownish limestone” of Savage, 2019) exhibits an increasing number of conodonts and pelagic ostracods. The lithology of the next unit (*triangularis* Zone, MS-D17), which overlies the UKW Horizon, exhibits few lithological differences from the limestone unit below (Fig. 7B).

In brief, facies analysis of the MS section reveals no fundamental differences. The combination of the overall slightly argillaceous lithology (see Fig. 12 and Appendix 2 for chemical data) and the lack of terrigenous grains, neptunian dykes, hardgrounds, and Fe/Mn crusts as well as of faunal elements, suggests a pelagic facies setting for the entire succession (for more detailed facies analysis, see Königshof et al., 2012).

4.2. Thong Pha Phum

In contrast to the monotonous composition of the pelagic limestone of the MS section, microfacies analysis of the TPP site reveals more differences in facies. The sediments are similarly poorly sorted, the fossil debris occurs in a micritic matrix, and macrofossils are rare in the entire section. Microfacies are generally characterized by poor faunal content (except some layers in which conodonts are numerous) and dominated by benthic ostracodes and trilobites, whereas tentaculitids, bivalves, and echinoderms are less frequent (see Fig. 6). Pelagic ostracodes are present in some beds. In terms of conodont biofacies, the TPP faunas are more dominated by shallow-water polygnathids (e.g., *Polygnathus decorosus*) in comparison to the MS succession (Savage et al., 2006, Table 1). Microfacies analysis enabled three microfacies to be distinguished, as follows:

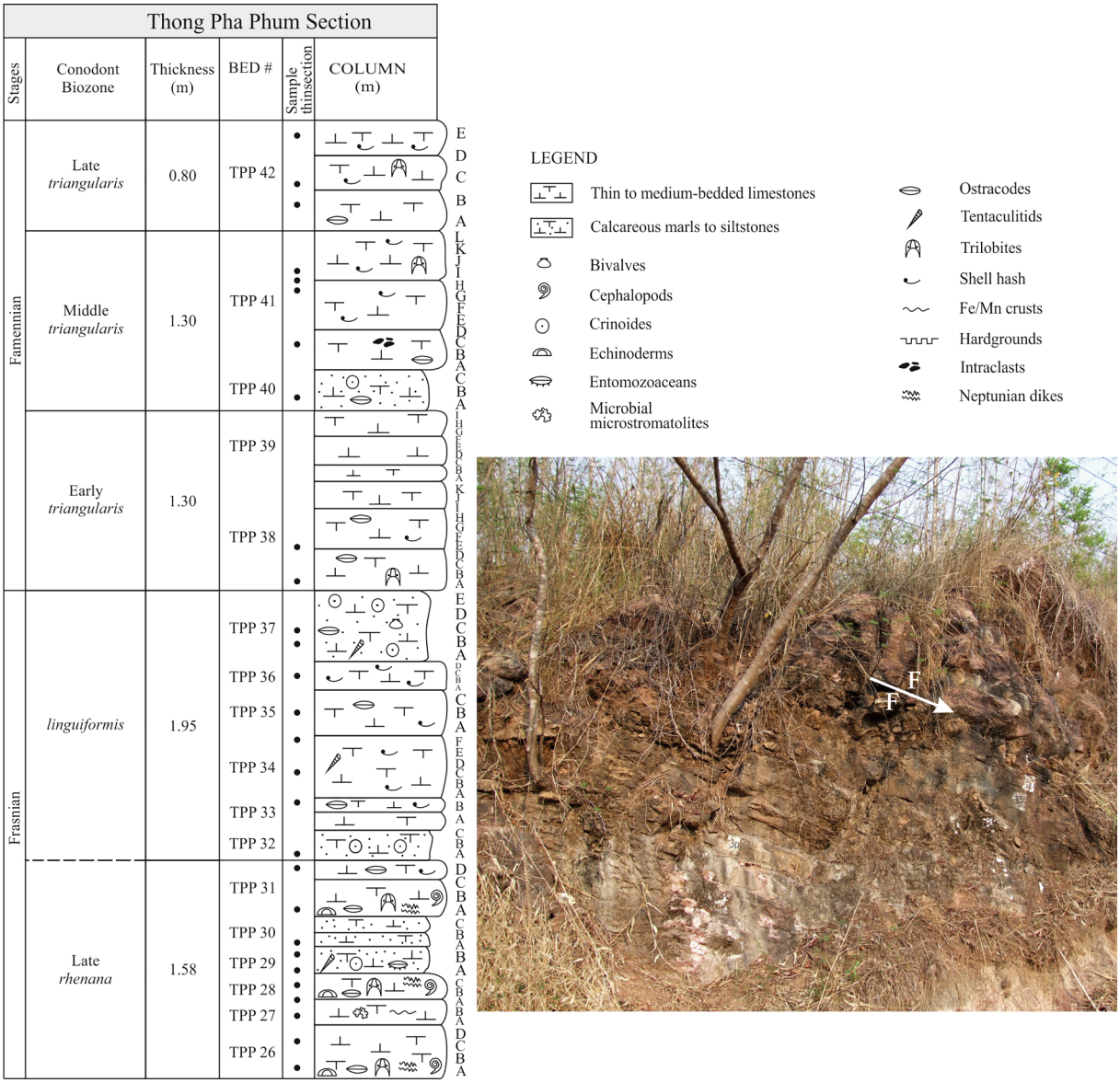

Fig. 6. Lithological and paleontological characteristics of the Thong Pha Phum section (for more refined petrologic classification, see Fig. 13) and field view of the locality. Arrows mark the position of the F-F boundary (numbers refer to the beds in TTP).

MF 1: Microbioclastic lime mudstone to wackestone

The measured section starts with microbioclastic lime mudstone to wackestone. This microfacies is characterized by thin to medium-bedded reddish limestone and is generally observed in the Late *rhenana* and *linguiformis* Zones (samples TPP 26A–28A, 31A). Fossils are composed of benthic ostracodes which are mainly disarticulated, conodonts, trilobite remnants, rare echinoderms, goniatites, and thin-shelled bivalves, scattered in a micritic matrix. A mottled/nodular fabric occurs, along with styliolitization, but is less frequent. Some parts of the limestones exhibit incipient dolomitization, but this feature is not very common in the entire section. The fossil content generally varies between > 5% and 15%, whereas neptunian dikes exhibit a more diverse fauna, with fossil content reaching 30% (Fig. 7C). The infilling sediment is composed of wackestone to packstone and contains slightly different fossils. Echinoderms, ostracodes, and gastropods are common; trilobites are less frequent. Internal brecciation is a common feature in some parts of the reddish limestone, ultimately leading to stylobreccia. The clasts are separated by clay seams. Occasionally, lithoclasts show ferruginous coating. The size of the clasts is variable, as is the degree of rounding, caused by burial solution rather than by transport. Ostracode shells are frequently dissolved and filled with sparry calcite. Fe-Mn crusts and microstromatolites are observed but occur with less frequency.

In thin-to-medium-bedded bed number 29A, the fossil content increases by as much as 10% and is composed exclusively of pelagic/hemipelagic fossils. An increasing number of pelagic fossils are pelagic ostracodes (entomozoaceans, Fig. 6D) or tentaculitids. This facies type represents a subfacies of MF1. Occasionally, hardground lithoclasts occur. Echinoderms are very rare. Crinoid ossicles are less frequent and exhibit canal patterns known from *Cupressocrinites*. In comparison to other fossils observed in this facies type, the crinoid ossicles are much larger and occur in this particular layer.

Interpretation: The overall fine-grained sediment and fossil content suggest a hemipelagic facies setting. Fossils found in Neptunian dykes indicate, to a greater extent, shelf paleoenvironments (e.g., echinoderms, gastropods).The lithoclasts occurring here often exhibit mineralizations such as ferruginous coatings and are interpreted as hardground lithoclasts (e.g., Burkhalter, 1995; Préat et al., 2000; Reolid et al., 2008; Reolid and Nieto, 2010; Zatoń et al., 2012; Lazar et al.,

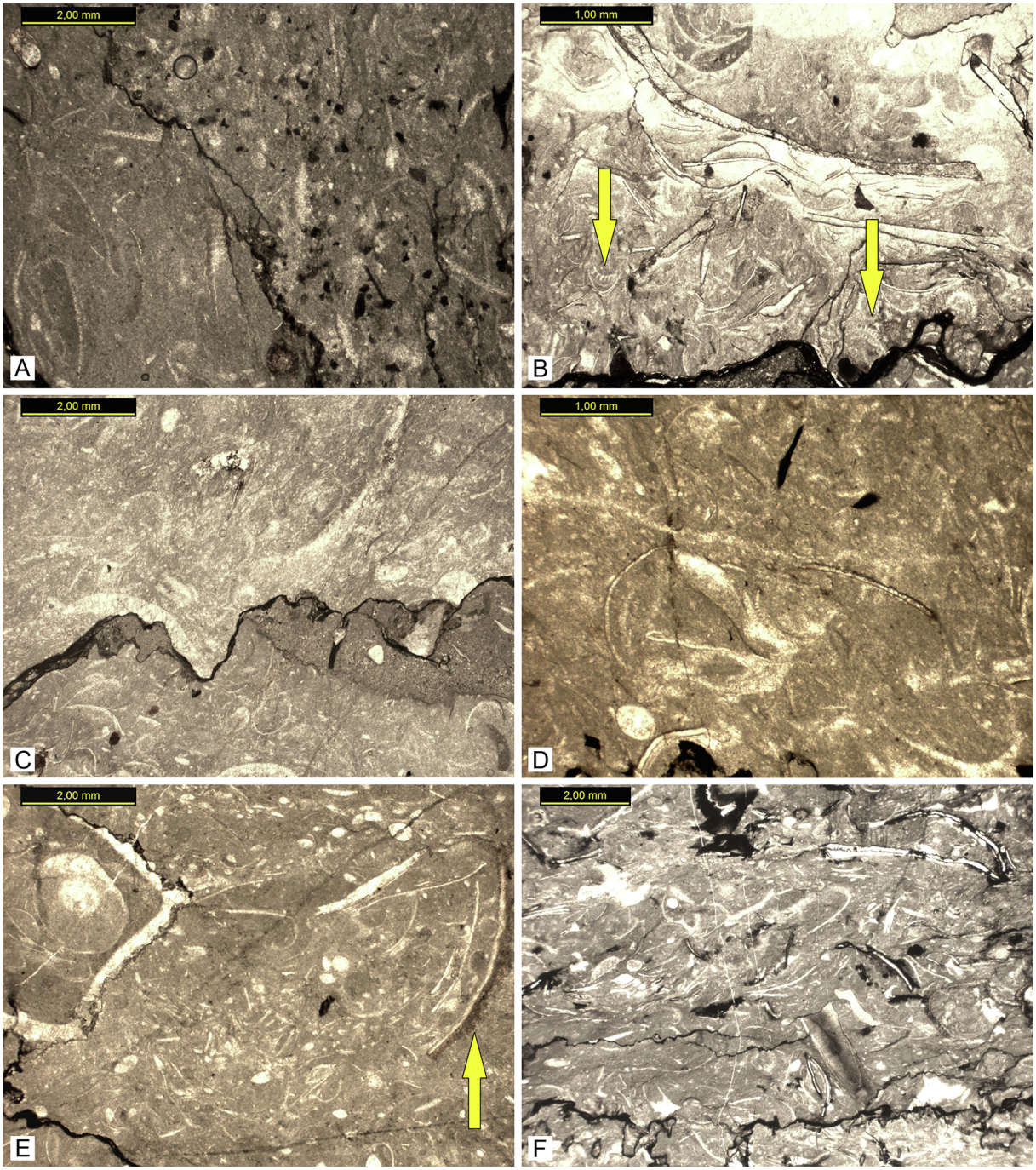

Fig. 7. Microfacies of the F-F boundary limestone beds at Mae Sariang (MS) and Thong Pha Phum (TTP). A: Microbioclastic wackestone shortly before the F-F boundary: sample MS-D18-A (*linguiformis* Zone). B: Microbioclastic wackestone: sample MS-D17 (*triangularis* Zone). C: Neptunian dykes composed of a rich and diverse fauna in comparison to the host rock: sample TPP 27A (Late *rhenana* Zone). D: Bioclastic wackestone with an increasing number of entomozoaceans: sample TPP 29A (Late *rhenana* Zone). E: Microbioclastic peloidal calcisiltite, sample TPP 36C (*linguiformis* Zone). F: Bioturbated bioclastic wackestone with rounded micritic intraclast: sample TPP 42B (Late *triangularis* Zone).

2013). These features, as well as the Mn-Fe crusts occurring here, are indicative of condensed hemipelagic limestone with low sedimentation rates, and suggest a slope environment. The occurrence of pelagic entomozoaceans is restricted to distinct layers. Variable fabric ranging from thin-bedded to nodular/mottled can be explained as a result of bioturbation in a low-energy environment. Large crinoid ossicles and hardground lithoclasts are interpreted as reworked material. As shown by Gingras et al. (2004), bioturbation promotes selective dolomitization, which occurs frequently in this facies type.

MF 2: Microbioclastic peloidal calcisiltite

This facies is characterized by grey limestone to calcareous marl and siltstone (peloidal calcisiltite, Fig. 7E). The latter ones occur in some layers (calcareous marl/siltstone in UKW bed 37; see geochemical data below). (Fig. 7E). This sediment type occurs in samples TPP 29B–30C, 32A–37C, and 41D. Fossil content is generally low (up to 5%) and is composed of ostracodes, trilobites, and rare tentaculitids. Occasionally, the fossil content can reach up to 10% in distinct layers. In samples TPP 36B and 37B, fossils are very rare (< 1%). Only ostracode shells occur.

In the overlying sample the sediment is the same, but the quantity of ostracodes is greater (up to 2%). Some layers are composed of microspar at the base, grade upwards to micrite, and exhibit millimeter-scale gradation. Light layers contain angular quartz grains. Fe-Mn nodules and fissures occur, along with burrows, but the latter are less frequent.

Interpretation: This microfacies occurs predominantly in the upper part of the Late *rhenana* Zone and the upper part of the *linguiformis* Zone as well as in one small layer in the *triangularis* Zone. Based on its rare fossil content and silt-sized grain size, a distal shelf position seems likely. Graded bedding, which occurs particularly in the Middle *triangularis* Zone (sample TPP 41D), indicates the deposition of sediments by distal turbidites, which may be associated with a major transgression marking the base of a third-order sequence (Johnson et al., 1985; Over, 2002).

MF 3: Bioturbated bioclastic wackestone

This microfacies forms the more medium- to thick-bedded limestone (particularly in samples TPP 38A–41C) in the upper part of the section. Even if some layers of the upper sequence belong to MF 1 and 2, most of the limestones of the Early to Late *triangularis* Zone are composed of reddish carbonates of MF 3. The number of fossils is very stable, up to 10%; trilobites and benthic ostracodes (some disarticulated, some complete) are the fossils predominantly observed. Occasionally, eroded and redeposited clasts occur (Fig. 7F); some of them are derived from shallower environments, such as small crinoids and brachiopod remnants, but occur in certain particular layers only. In contrast to MF 1, bioturbation is well developed in this medium- to thick-bedded limestone, as shown in Fig. 7F. Ferruginous crusts and hardgrounds occur, but are not as prominent as in MF 1.

Interpretation: The MF 3 is characterized by reduced sedimentation rates in a well-aerated slope environment. Bioturbation is the most prominent feature. All in all, this facies type is very similar to Austria's reddish Adnet limestone, which is interpreted as a slope environment below the photic zone (e.g., Böhm et al., 1999).

5. Carbon isotope stratigraphy (Racki)

Both Thai successions reveal a more (MS) or less (TPP) distinctive positive $\delta^{13}C$ excursion near the F-F boundary, with a major spike in the basal Famennian (Early *triangularis* Zone; Fig. 8) and a peak value of 4.1‰ at MS. A more gradually decreasing shift to the Upper Devonian baseline (1.5‰) occurring in the Middle *triangularis* Zone at MS (see also Fig. 3 in Savage, 2013, showing a negative one-point excursion in the basal Famennian in the tectonically repeated slice) is diachronously recorded. At TPP, the $\delta^{13}C$ highstand plateau persisted almost to the top of the *triangularis* Zone. Furthermore, an unique precursor of a positive spike is noted near the middle of the *linguiformis* Zone at this locality. Also within the Late *rhenana* Zone, a highly positive $\delta^{13}C$ trend (above 4‰) is recorded in several samples at the base of the TPP section, as well as in relic form (2.6‰) at MS.

Therefore, as concluded by Savage et al. (2006), Königshof et al. (2012), and Savage (2013), the global Upper Kellwasser $\delta^{13}C$ positive excursion, known from the F-F passage beds of Europe, North America, China, and elsewhere, is clearly manifested in the Thai sections (Figs. 8 and 9), as well as in northern Vietnam (Komatsu et al., 2019). On the

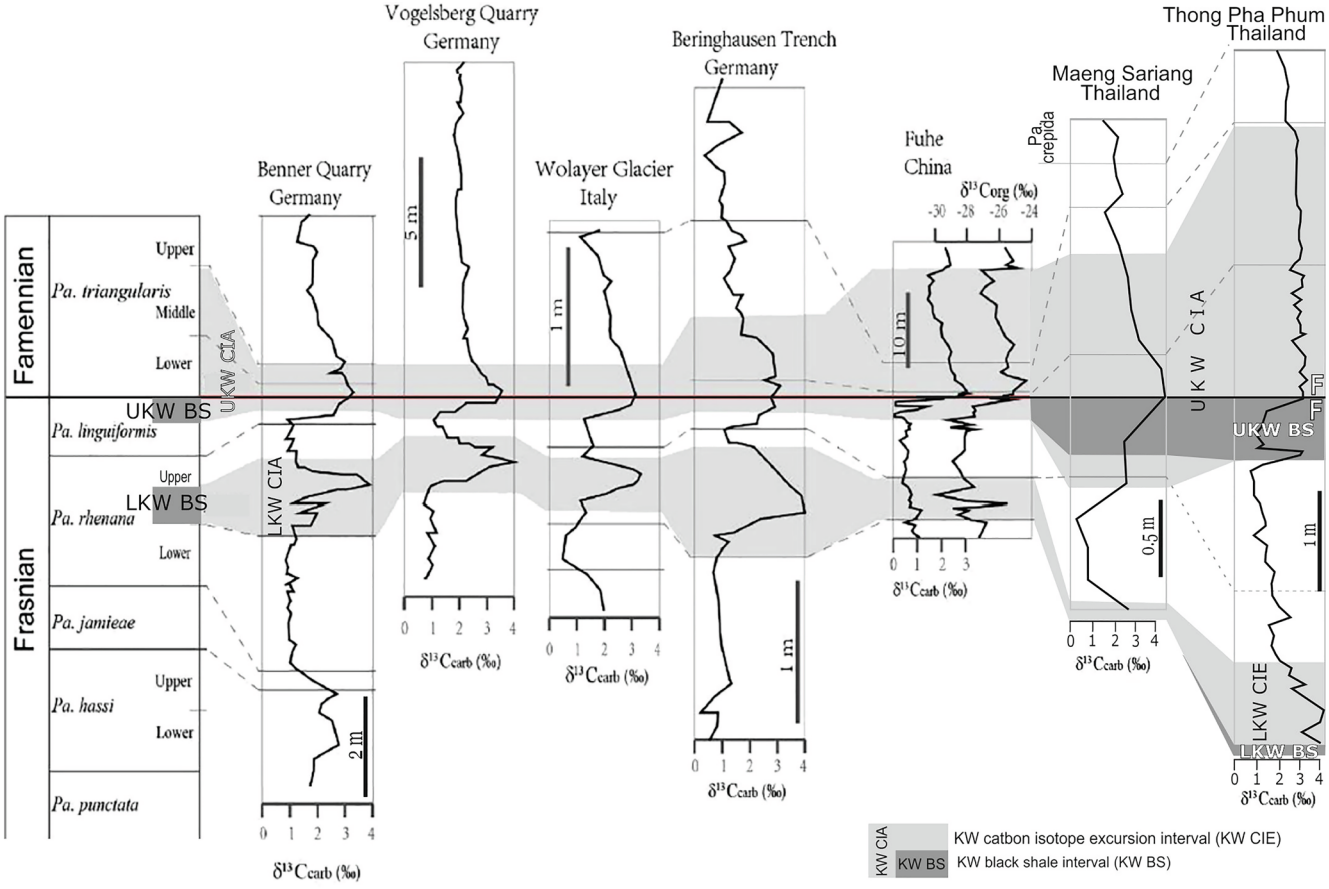

Fig. 8. Bio- and chemostratigraphic correlation of Thai carbon isotope profiles (after Savage et al. 2006; Savage, 2013) near the F-F boundary with standard German and Chinese sections. Carbon isotope data of the European localities are derived from Buggisch and Joachimski (2006), the Fuhe and Dongcun data from Chen et al. (2013) and Xu et al. (2012), respectively (modified Fig. 10 from Chang et al., 2019; see also Fig. 11 in Huang et al., 2018b). Note the differentiation between the KW black shale intervals (= "global anoxic events"; KW BS) and anomalous $\delta^{13}C$ excursions (KW CIA, as defined herein) shown for the Thai successions.

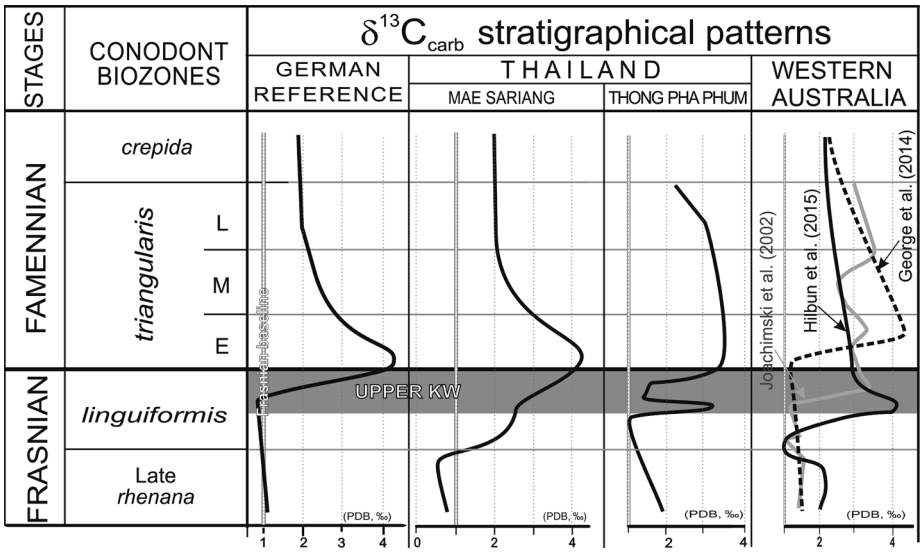

Fig. 9. Schematized carbon isotope time series of F-F boundary beds from Central Europe (Joachimski and Buggisch, 1993, 2002), both Thai localities, and Western Australia (Canning Basin; cf. Fig. 8). The overall similarity of the more condensed MS signature to the global standard is noteworthy, as is a peculiarity of the TPP $\delta^{13}C$ profile closely comparable to previously reported "atypical" Australian signatures (see also more standard $\delta^{13}C$ curves from the region in Stephens and Sumner, 2003). The Frasnian baseline value is based on Joachimski et al. (2002; see Fig. 1).

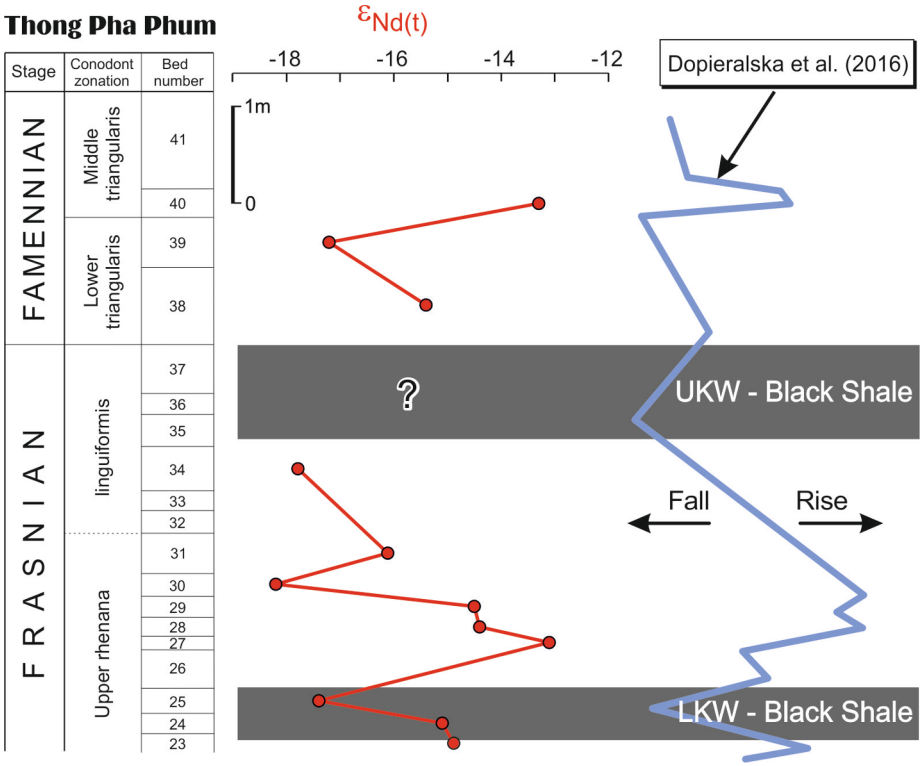

Fig. 10. Variation of $\varepsilon_{Nd(t)}$ values in Late Devonian conodonts of the Thong Pha Phum section compared to the eustatic sea-level curve (in blue) inferred from Nd isotope data of seawater in the Variscan realm (adopted from Dopieralska et al., 2016). Dark gray bands show the positions of Kellwasser black shaly units (LKW, UKW) in the Upper Devonian of Germany. Note that geochemical data for beds 23–25 were limited during the current study to Nd isotopes only. (For interpretation of the references to colour in this figure legend, the reader is referred to the web version of this article.)

other hand, conversely with respect to the overall standard, and notwithstanding the more condensed $\delta^{13}C$ signature at MS, the TPP isotopic curve shows marked deviations from the German reference of the main KW event (Fig. 9). In this respect, the latter chemostratigraphic pattern combines features known only from the Western Australian $\delta^{13}C$ curves, which are extraordinarily unstable on a regional scale, presented from the Canning Basin by Joachimski et al. (2002), George et al. (2014), and Hillbun et al. (2015). The positions of peak $\delta^{13}C$ values are evidently diachronously and/or irregularly recorded, at least in the Australian F-F sections, in contrast to a stable basalmost Famennian maximum recorded following a consequent positive shift in the German reference successions (Fig. 9). In addition, due to an increasing number of more or less "odd" $\delta^{13}C$ temporal patterns from China and Canada, the KW chemostratigraphic standard has recently

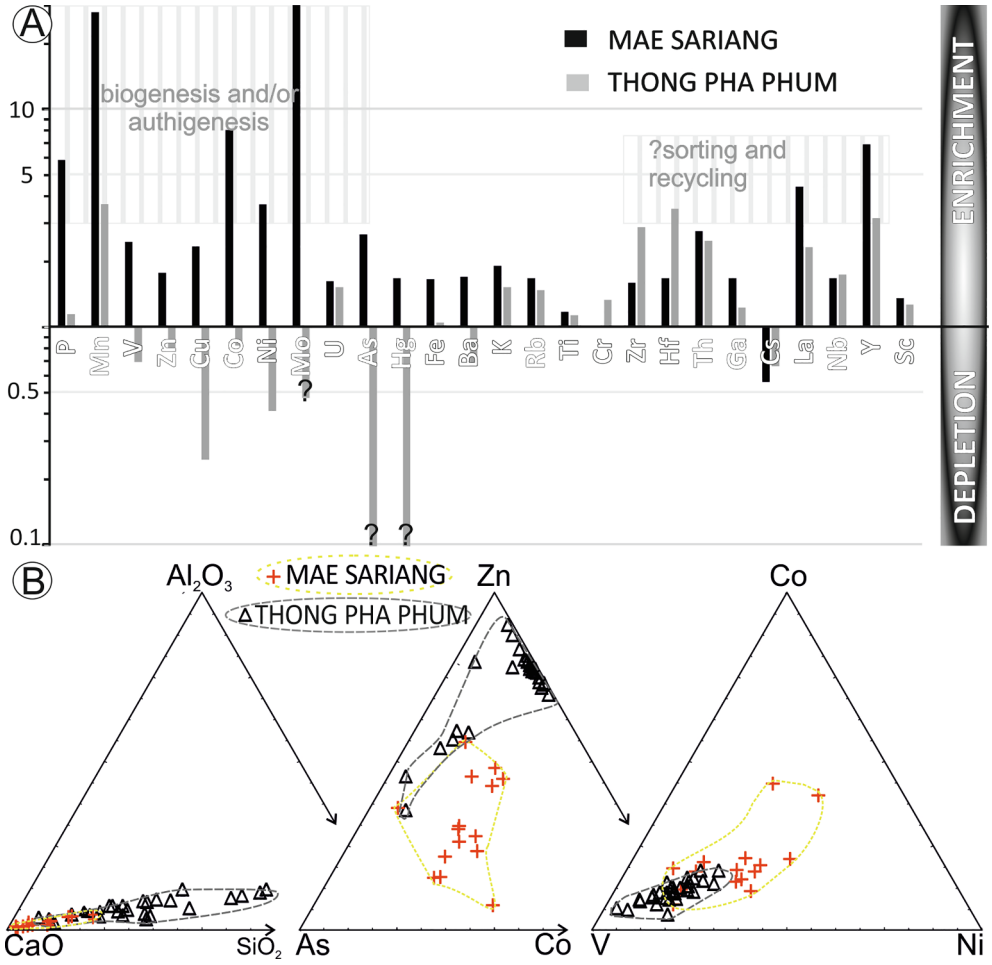

Fig. 11. A Enrichment factors for selected elements from both Thai sections used in the estimation of environmental proxies (Figs. 12–20) and their conjectural genetic implications for the substantial (greater than threefold; see Riboulleau et al., 2018) enrichment values of two major element suites. Samples were normalized using the average of post-Archean Australian shale (PAAS) compositions (Taylor and McLennan, 1985), supplemented by data for Hg and As from Wedepohl (1991). Question marks show uncertainty regarding the actual depletions at TPP for Mo, Hg, and As, due to dominant values below the detection limit (see Table 1). B: Ternary plots of Al_2O_3–CaO–SiO_2, Zn–As–Co, and Co–V–Ni for TPP and MS, illustrating the essential difference in element distributions between the two Thai sections.

been contradicted by Whalen et al. (2017), Chang et al. (2019), and especially by Carmichael et al. (2019). For an extreme example, in the deep-water carbonate-biosiliceous succession at Nandong, South China, the positive UKW excursion is limited to the *linguiformis* Zone, while negative $\delta^{13}C$ shifts characterize the LKW interval (Huang et al., 2018b, Figs. 3 and 11). Thus, the need for terminological refinement is obvious (as shown in Figs. 8–10) in relation to:

1. the KW black shale (KW BS) level (=KW anoxic event *sensu stricto*), corresponding generally to the lower (=rising) half of KW $\delta^{13}C$ excursions (Joachimski and Buggisch, 1993, 2002; see Fig. 1), and to the precisely defined intervals of conodont zones in terms of global anoxic events (e.g., Walliser, 1996; Becker et al., 2012; see Fig. 1). This worldwide status of permanent anoxia has been questioned many times (e.g., Racki et al., 2002; Ma et al., 2016; Song et al., 2017; Chang et al., 2019; see review of the models in Crasquin and Horne, 2018; Carmichael et al., 2019), especially in these Western Australian domains (e.g., George et al., 2014; Hillbun et al., 2015; Tulipani et al., 2015).
2. the KW carbon isotope excursion (KW CIE) interval (=KW event *sensu lato*): the certain diachronous timespan of all KW $\delta^{13}C$ excursions (Fig. 8; see also Joachimski et al., 2002; Buggisch and Joachimski, 2006; Whalen et al., 2015, 2017; Ma et al., 2016; Huang et al., 2018b; Chang et al., 2019). The intervals in the Thai sections were clearly determined by $\delta^{13}C$ values above the Frasnian baseline, traditionally assumed to be 1‰ (see Figs. 1 and 9), although the revised European data of Buggisch and Joachimski (2006, Fig. 7) suggest a slightly higher value for the Upper Devonian.

Such large-scale local variations in $\delta^{13}C$ time series had been previously recorded from Ordovician epeiric seas (Panchuk et al., 2006). Intra-regional biogeochemical modifications may indicate enhanced lateral variability in the intensity of primary production and biological pumping (sea-water aging; Panchuk et al., 2006; Immenhauser et al., 2008; see also Huang et al., 2018b). In addition, prominent inter-regional differentiation of chemostratigraphical $\delta^{13}C$ patterns is also well known, e.g., for the Middle Frasnian *punctata* Event (Pisarzowska and Racki, 2012). In the context, oceanic $\delta^{13}C$ values may also be markedly different than these commonly presented for Paleozoic carbonate shelves (Brand et al., 2009). In Silurian pelagic regimes, $\delta^{13}C$ excursions are extraordinarily negligible (see discussion in Loydell, 2007), confirming the main burial loci of organic carbon in shallow-water settings, Brand et al. (2009, Fig. 4) quoted an unusually highly positive $\delta^{13}C$ value (above 4‰) for Middle Devonian open-ocean brachiopod calcite from south China. In the Thai sections, however, the $\delta^{13}C$ time series of pelagic sediments at MS agrees overall with the German chemostratigraphic "standard," whereas a distinctly lower amplitude of the F-F excursion (below 1.5‰) occurs at TPP. Varying degrees of geochemical decoupling from the global ocean may occur in semi-restricted epeiric basins (see Dopieralska et al., 2006; Brand et al., 2009), thus allowing regional C-cycling processes to modify the global $\delta^{13}C$ signal through the local transfer of weathered carbonate and sedimentary organic matter.

To sum up, the UKW evidently occurs at TPP (Figs. 8, 9 and 16) and at least partly corresponds to the UKW BS level. The upper part of the LKW $\delta^{13}C$ excursions is also evidently recorded at this site, whereas the LKW BS interval is implied for the underlying beds (based on Nd isotope data; Fig. 10), which, unfortunately, have not been studied in terms of

elemental geochemistry. At MS, only the top interval of the LKW CIE interval can be assumed for the lowermost samples (see Figs. 8 and 15). In addition, surprisingly, the UKW CIR may extend downward as far as the *rhenana* Zone. The upper limit of the UKW-related $\delta^{13}C$ excursion, indistinct in both localities, may be placed either in the Middle *triangularis* Zone (Fig. 8) or higher in the successions; thus, only the LKW CIE and UKW BS intervals are marked in the figures below. Altogether, conversely to the oxygen isotope data ($\delta^{18}O$ between −21 and −13‰ at MS; cf. Savage et al., 2006 for TPP), the secular $\delta^{13}C$ variation in both Thai successions points to their overall representative character, so important in event-stratigraphical analysis. This temporal framework, despite several possible factors biasing the global event record, suits the requirements for more detailed environmental interpretation in the key biodiversity crisis interval with the use of other geochemical proxies.

6. Nd isotopes: geotectonic and eustatic signals (Belka and Dopieralska)

Dopieralska et al. (2012) used conodonts collected from the Thong Pha Phum and Mae Sariang sequences to reconstruct the neodymium isotope composition of seawater in western Thailand during the Late Devonian. At Thong Pha Phum, the conodonts were characterized by very low $\varepsilon_{Nd(t)}$ values (between −13.1 and −18.2) and very high Sm/Nd ratios (between 0.36 and 0.66). In contrast, the conodonts from the Mae Sariang section yielded signatures that were much more radiogenic, with $\varepsilon_{Nd(t)}$ values ranging from −8.7 to −11.1 and uniform, low Sm/Nd ratios (between 0.20 and 0.23). The extremely low $\varepsilon_{Nd(t)}$ values at Thong Pha Phum have been interpreted to reflect a passive margin continental setting and a paleogeographic position very close to a continental area where Paleoproterozoic and Neoarchean rocks were eroded. In addition, Dopieralska et al. (2012) pointed out that strong temporal variations in ε_{Nd} (see Fig. 10), along with very high Sm/Nd ratios, suggest the sequence's proximal location on the shelf, at a relatively short distance from the coast. Consequently, they postulated that, during Late Devonian times, the Sibumasu Terrane was situated near the Archean cratons of Western Australia and was more likely attached to the Australian continental crust. In contrast to the TPP site, the seawater at Mae Sariang, characterized by more radiogenic signatures and low Sm/Nd ratios, resembled present-day oceanic waters. Therefore, the MS sequence was interpreted as having been deposited on an isolated submarine height located within the Paleotethys Ocean (Dopieralska et al., 2012; cf. Königshof et al., 2012).

Unfortunately, conodonts are virtually absent or extremely rare in the uppermost Frasnian interval of the TPP section (Savage et al., 2006). Consequently, the *linguiformis* Zone is not sufficiently constrained by biostratigraphy. This is also the reason it was impossible to carry out Nd isotope measurements of conodonts for the entire TPP sequence. Although fragmentary, the Nd isotope curve exhibits very strong variations in $\varepsilon_{Nd(t)}$ values (Fig. 10), which suggests that eustatic sea-level changes exerted a major influence on carbonate deposition. Several studies have shown that eustasy appears to be the main factor governing rapid temporal changes in the Nd-isotope composition of seawater on the shelves (Dopieralska, 2003; Holmden et al., 2013; Hughes et al., 2015; Dopieralska et al., 2016), although variations in ε_{Nd} values may also result from changes in paleogeography, seawater circulation, paleoclimate, or volcanism (Dopieralska, 2009; Dera et al., 2015). Because regressions accelerate erosional processes and usually provoke an enhanced supply of non-radiogenic Nd to the ocean, they cause declines in ε_{Nd}. Consequently, transgressions are responsible for positive shifts in the ε_{Nd} values of seawater. Eustatic variations are more strongly expressed in ε_{Nd} close to the coast and become very weak in distal, pelagic settings. Very recently, Dopieralska et al. (2016) constructed an eustatic sea-level curve for the late Frasnian–early Famennian period, inferred from temporal trends in ε_{Nd} values identified in Devonian sequences of the Variscan realm. The fluctuations in $\varepsilon_{Nd(t)}$ values identified in the TPP sequence trace almost perfectly some fragments of the eustatic curve, especially in the interval of the Upper *rhenana* Zone (Fig. 10). Clearly visible in the TPP curve are both the regressive shift related to the Lower KW level and the subsequent transgression. Hence, it is apparent that beds 23–26 (in part) of the TPP section represent an interval equivalent to the Lower Kellwasser black shale/limestone in Germany (see Figs. 1 and 8). A positive shift in $\varepsilon_{Nd(t)}$ values between beds 39 and 40 appears to coincide with a transgressive pulse in the Nd sea-level curve, as well as with a deepening event identified in various regions of Euramerica at the base of the Middle *triangularis* Zone (Johnson et al., 1985).

7. Inorganic bulk geochemistry and evaluation of environmental changes (Racki and Pisarzowska)

The event-chemostratigraphic study is based on conventional analyses of whole-rock bulk samples, which is the current research standard in sedimentary geology (see reviews in Arthur and Dean, 1991; Sageman and Lyons 2003; Tribovillard et al., 2006; Calvert and Pedersen, 2007; Ramkumar, 2016; Craigie, 2018). More refined analyses of separate carbonate and non-carbonate (detrital) phases are rarely applied (Wedepohl, 1971; Kiipli et al., 2012; see also the approach of Śliwiński et al., 2012), in part because the chemistry of the carbonate phase is particularly affected by "changes in post-depositional diagenesis that are unrelated to syn-depositional processes" (Craigie, 2018, p. 104; see also review in Swart, 2015; Hood et al., 2018). To compare geochemical proxies in sediments with fluctuating carbonate dilution, the trace element is usually normalized to the aluminum values. As summarized by Tribovillard et al. (2006, p. 15), Al normalization "cannot be relied on alone to identify and quantify contributions by sediment components other than the detrital fraction (Van der Weijden, 2002)". In fact, most of the chemostratigraphic studies in carbonate successions are based on a non-carbonate, largely aluminosilicate phase (see below).

The elemental multi-proxy approach to interpretations of key environmental factors is routinely used in the case of carbonate-dominated successions of the eventful KW Crisis interval, with emphasis on redox-state tracers, as exemplified by George et al. (2014), Joachimski et al. (2001, 2009), Lash (2017), Pujol et al. (2006), Racki et al. (2002), Riquier et al. (2006), Riboulleau et al. (2018) and Weiner et al. (2017), among others.

7.1. General comparative characteristics of Thai successions

In terms of chemical composition (Figs. 11 and 12; Table 1), the Mae Sariang succession is characterized by a much greater number of monotonous limestone lithologies (in accordance with the microfacies data; see above). Calcium carbonate content (calculated from CaO) is above 85%, with a major exception in the basal part, where the clay admixture may exceed 10% (Al_2O_3 contents up to 2.6%). In most samples, the potential quartz contribution is rather minor (with an average SiO_2 value of 4.8% and a maximal value of 12.1% in the lowermost sample; see Fig. 12). Dolomitization also remains unimportant in the succession, as MgO content is below 0.8% (on average, 0.5%), and linked with aluminosilicates (r = 0.88 with Al).

At Thong Pha Phum, the content of siliciclastic admixture is increased threefold, and $CaCO_3$ values are generally less than 80% (Fig. 13). Calcareous marls (with clay content above 25%) dominate in the middle segment of the succession (Al_2O_3 values above 5%). Moreover, SiO_2 values frequently exceed 20% (maximally almost 44%), and the sandy character of the marly deposits is evident in the Frasnian part of the section. In two of the highest Frasnian samples, SiO_2 concentrations exceed even calcium carbonate content. Therefore, in strictly petrographic terms, limestones *sensu stricto* are absent from the locality. As at MS, MgO contents alone, in 4 samples, amount to more than 1% (average 0.5%), but are less strictly correlated with siliciclastic

Table 1
Median concentrations of selected elements in the Thai sections under study, against the average limestone, average shale (PAAS; Hg and As from Wedepohl, 1971) and upper continental crust abundance levels (x – not determined); above ca. three-fold enrichment (in yellow) and depletion (in grey).

Element	Average limestone (Wedepohl, 1971, 1991)	Post Archean Australian shale (PAAS) (Taylor and McLennan, 1985)	Upper continental crust (McLennan, 2001)	Median content in **Mae Sariang**	Median content in **Thong Pha Phum**
MAJOR ELEMENTS (in weight percent)					
Al	1.03	10	8.04	0.43	1.8
Si	3.5	29.36	30.5	1.5	8.8
Ca	31.5	0.93	3.0	25.76	16.4
Mg	2.6	1.33	1.33	0.27	0.3
Fe	1.5	5.05	3.5	0.48	0.99
K	0.47	3.07	2.8	0.23	0.85
MINOR AND TRACE ELEMENTS (in ppm)					
P	300	700	700	260	170
Mn	700	900	600	1500	600
V	20	150	107	20	18.5
Zn	23	85	71	8	13
Cu	4	50	25	2.6	20.7
Co	2	23	17	6	3
Ni	15	55	44	11.5	4.2
Mo	0.4	1	1.5	0.2	<0.1
U	2.1	3.1	2.8	0.2	1
As	2.5	(10)	1.5	9.2	<0,5
Sb	0.3	x	0.2	0.4	<0.1
Hg	0.03	(0.4)	x	0.03	<0.01
Ba	120	650	550	59	78
Rb	11	160	112	11	43
Ti	400	6000	4100	360	1300
Cr	11	110	83	<20	25
Zr	19	210	190	18	119
Hf	0.3	5	5.8	0.4	3.5
Th	1.7	14.6	10.7	2.3	7.1
Ga	4	20	17	1.6	4.4
Cs	1	15	4.6	0.4	1.7
La	4.1	38	30	11.5	17.3
Nb	0.3	19	12	1.7	7.1
Y	3.8	27	22	11.7	17.1
Sc	1	16	13.6	1	4

material (r = 0.69 with Al), and therefore dolomite may occur in trace amounts.

Consequently, both Thai carbonate sections, even if described in the results of fieldwork as including limestones only (e.g., Savage et al., 2006; Dopieralska et al., 2012; Königshof et al., 2012), are in fact notable for their somewhat dissimilar lithologies (see Figs. 4 and 6); this disparity is also evidenced by the enrichment/depletion patterns in Table 1. When compared with the average limestone composition of Wedepohl (1970, 1991), the key lithophile elements are significantly abundant in carbonate-clay and partly-sandy sediments from TPP; these elements include Zr (by a factor of 6!, and even more for the related Hf), Ti, Cr, Rb and Th, as well as REEs; however, Cu, Ni, Mo, As, and Sb are notably depleted. Of course, purer limestones of the MS section are more typical in terms of chemical composition, even if values of Fe and U are markedly low and Cu and As are more abundant.

The Thai samples were normalized using the PAAS compositions, which are commonly preferred in the subject literature (Fig. 11). An enrichment factor (EF) above 3 is generally thought to indicate amplified abundance of a given element due to its biogenic or authigenic origin (as opposed to merely detrital affinity; see Riboulleau et al., 2018). This origin may be hypothesized for several elements in the MS succession, such as P, Mo, Co, Ni, and As (even if largely influenced by only two enormously enriched samples), as well as for Mn in both sections. In general, however, chalcophile and siderophile elements are depleted at TPP. In addition, some elements included in the lithogenous fraction (e.g., Y, La, and Th) also exhibit significantly high abundance levels at both sites, but more frequently at TPP (also Hf and Zr).

The REE concentrations in both sections are generally similar or lower than PAAS (see also Fig. 20). Sample D-18Aex/2011 from MS is characterized by higher REE concentrations, especially Dy, in comparison to the other samples. Research on modern (Webb and Kamber, 2000) and Devonian (Nothdurft et al., 2004; Franchi et al., 2016) microbialites revealed that they are characterized by the highest relative REE concentrations of co-occurring carbonates. Recent studies show that some bacterial species, e.g., *Escherichia coli* and *Bacillus subtilis* (Takahashi et al., 2005) and *Penidiella* sp. T9 (especially Dy; Horiike

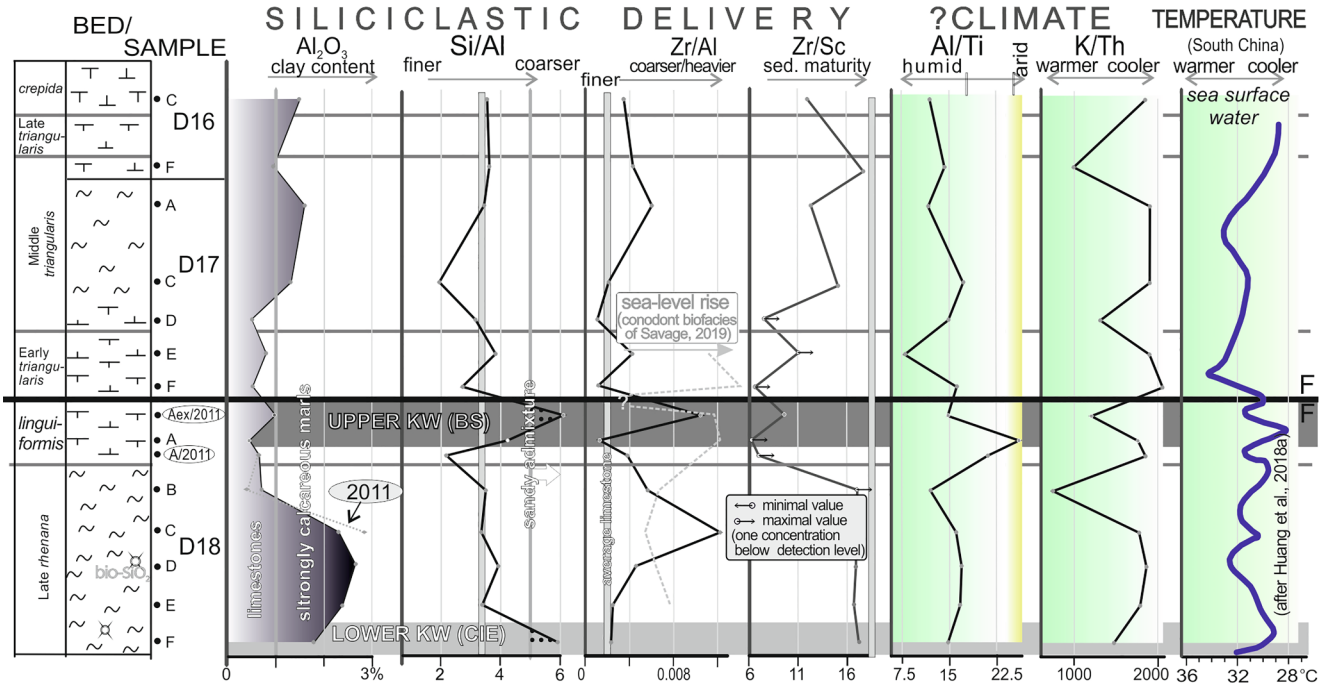

Fig. 12. Secular trends of selected geochemical proxies for terrigenous input and related putative indicators of sediment maturity/recycling and weathering/climate in the Mae Sariang section (for a detailed log, see Fig. 4), compared with sea-level changes revealed by conodont biofacies succession (after Savage, 2019, Fig. 3 therein) and sea surface water temperature based on $\delta^{18}O_{PO4}$ records of conodonts from South China shelf (Huang et al., 2018a, Fig. 7). Thin rectangular vertical lines indicate levels of the ratios calculated for average limestone after Wedepohl (1970, 1971, 1991). Results for clay content from the 2011 subsection are also shown (broken gray line) as probably supplementing the stratigraphic record of the top Frasnian bed D18 in the reference subsection. Note that only the Lower KW carbon excursion interval (CIE – see Figs. 8 and 15), not the LKW black-shale interval (BS), is recorded in this section, along with increased terrigenous delivery even in the transgressive setting of UKW (based on the conodont biofacies data of Savage, 2019, Fig. 3).

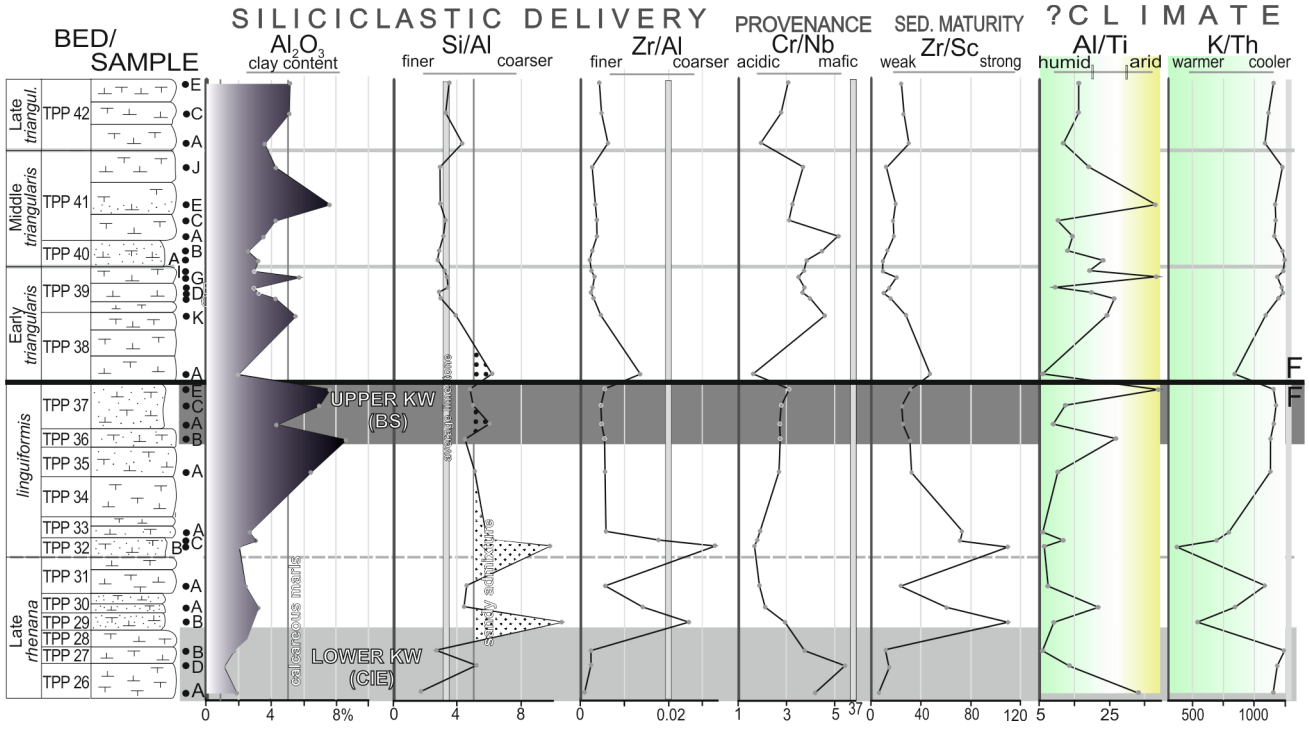

Fig. 13. Secular trends of selected geochemical proxies for terrigenous input and related putative indicators of provenance, sediment maturity/recycling, and weathering/climate in the Thong Pha Phum section (for a detailed log see Fig. 5; cf. Fig. 12; compare Figs. 14, 17 and 20). Note that only the Lower KW carbon excursion interval (CIE – see Figs. 8, 10, and 16), not the LKW black-shale interval (BS), is recorded in this outcrop.

and Yamashita, 2015), accumulated REEs from a solution. Therefore, the higher REE concentrations in sample D-18Aex/2011 from the extremely condensed terminal Frasnian layer (Figs. 4 and 5) may result from more intense REE uptake (especially dysprosium; Horiike and Yamashita, 2015) related to microbial biosedimentary activities (cf. Li et al., 2017), especially since hardgrounds and microbialites are often

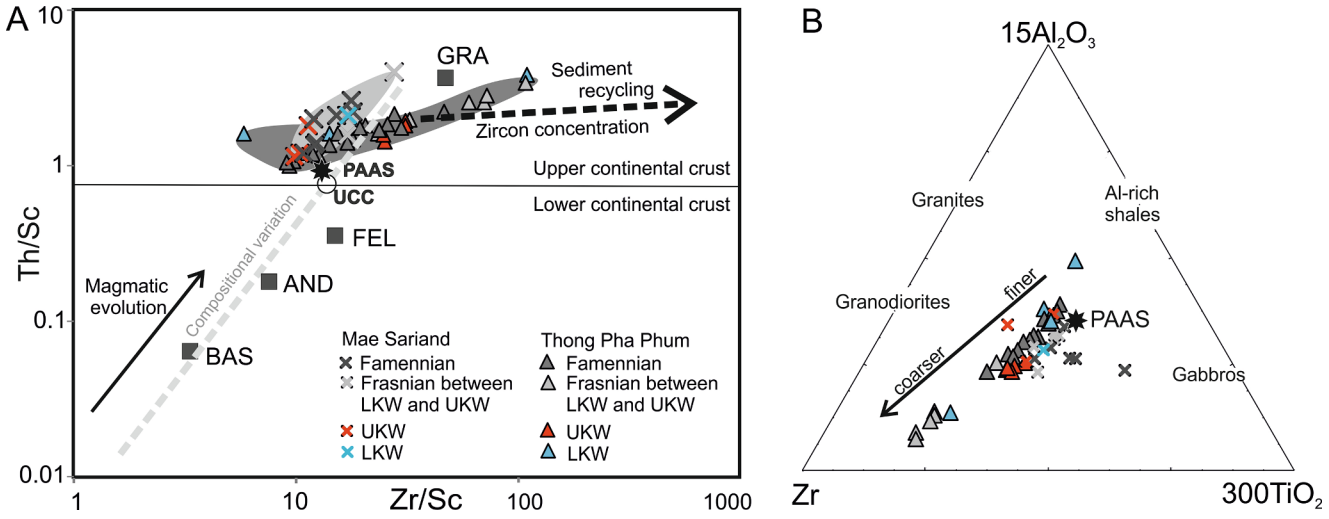

Fig. 14. (A) Th/Sc–Zr/Sc cross-plot and (B) ternary plot of $15xAl_2O_3$–Zr–300 × TiO_2 for the Thai successions, with clearly recorded felsic provenance and Zr enrichment due to advanced sediment sorting and recycling in the coarse-grained fraction, deposited during the Frasnian in the TPP (see also Figs. 12, 13 and 17). For comparison compositions (after McLennan et al., 1993) of average post-Archaean Australian shales (PAAS) and average upper continental crust (UCC) are shown, as well as average principal magmatic rock types (BAS – basalt, AND – andesite, FEL – felsic volcanic rocks, and GRA – granite, after Condie, 1993).

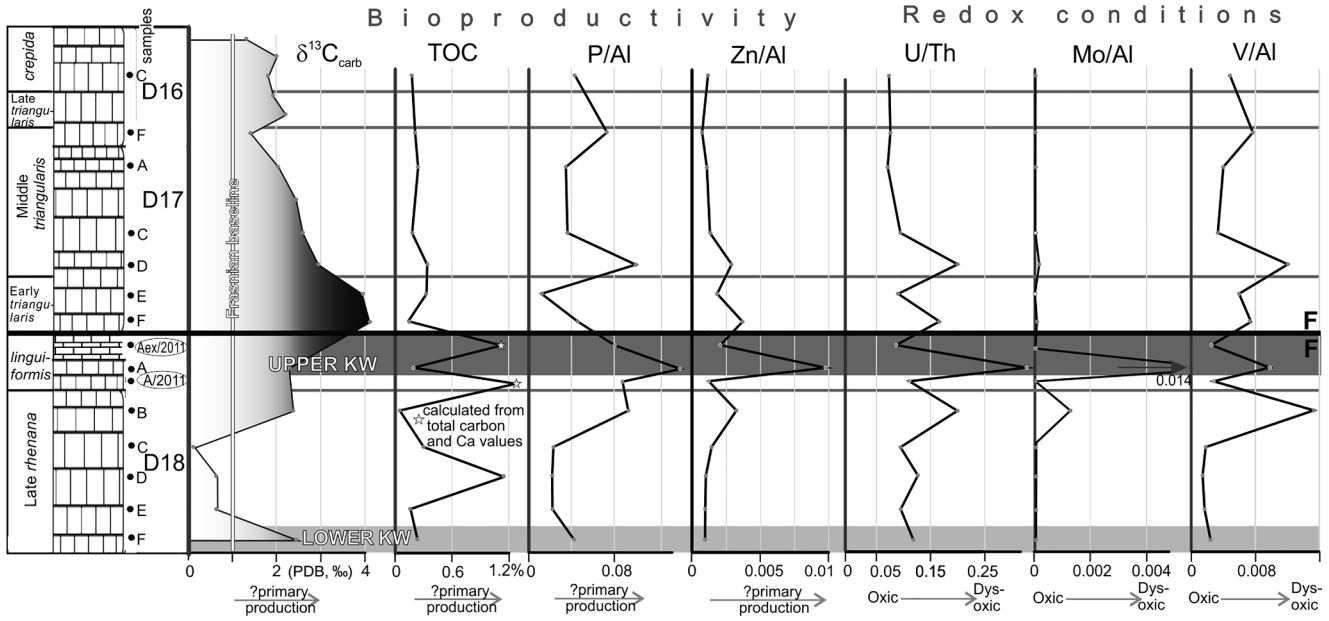

Fig. 15. Secular trends of selected geochemical proxies for redox conditions and bioproductivity in the Mae Sariang section (see also Figs. 8 and 12); $\delta^{13}C$ curve after Savage (2013, Fig. 3). Note two only approximated high TOC values in the topmost Frasnian interval.

related (Christ et al., 2015).

The introductory data are of essential importance in the environmental discussion below. Because Al is well known as a crucial immobile aluminosilicate tracer, and dilution effects by carbonate may be reduced with the use of element/Al ratios as weight ratios, selected Al-normalized ratios are considered relevant environmental proxies (e.g., Sageman et al., 2003; Pujol et al., 2006; Calvert and Pedersen, 2007; Ver Straeten et al., 2011). This normalization is reasoned for the Thai samples on the basis of the relatively small variation in Al concentrations (see discussion in Van der Weijden, 2002, and Tribovillard et al., 2006), but not applied to authigenic elements such as Mo and As. However, if (1) the non-normalized element concentrations are generally similar to the average limestone contents, and (2) connected, with a close correlation between the element and Al, the ratios cannot be considered an environmental fingerprint; these two characteristics clearly determine its dominance by terrigenous provenance and scarcity of the authigenic or biogenic fraction (Tribovillard et al. 2006; Racki et al., 2012; Śliwiński et al., 2012; Riboulleau et al., 2018; but see Fig. 17). For example, conversely to Ba values in particular, Al-normalized phosphorus concentrations are frequently usable in a bioproductivity context (e.g., Racki et al., 2012). Of course, the selection of the proxies shown in Figs. 12–20 was also constrained by their constituent values (mostly) below detection levels, which excluded some proxies (e.g., the crucial Cr at MS). On the other hand, spikes limited to a single sample (one-point) are common in the more (MS) or less (TPP) condensed stratigraphical records of both sections (see Fig. 8), despite their relatively dense sampling (at intervals of 10–25 cm).

7.2. Terrigenous input

The total lithogenous fraction content of carbonate rocks, as an approximation of terrigenous, essentially siliciclastic input, is mirrored by Al concentration, whereas aeolian delivery can be detected using elemental indicators for sediment grain-size, such as Si/Al and Zr/Al

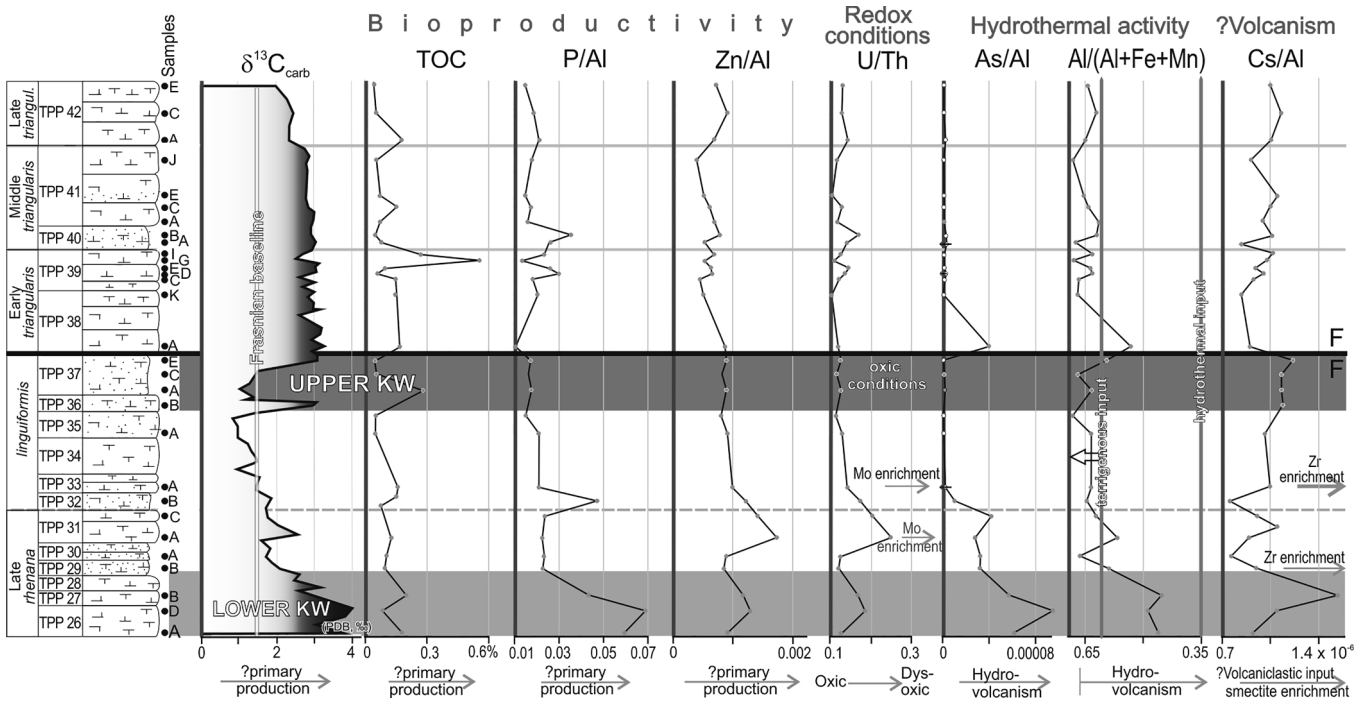

Fig. 16. Secular trends of selected geochemical proxies for redox conditions, bioproductivity, and volcanic/hydrothermal processes in the Thong Pha Phum section (see also Figs. 8, 12 and 13); $\delta^{13}C$ curve after Savage et al. (2006, Fig. 4).

ratios (Calvert and Pedersen 2007; Ver Straeten et al. 2011). The applicability of the phase ratios of quartz to aluminosilicate (clay) is justified by their strong positive correlation (r = 0.91 and 0.74 at MS and TPP, respectively), coupled with the negligible occurrence of biogenous silica shown by microfacies data (but see below the data for MS, Fig. 17). In particular, larger average grain size is tracked by elevated Zr/Al and Si/Al ratios, recording proportionally increased contents of zircon and quartz grains, respectively. The ratio of Zr/Sc is used as an indicator of the maturity of detritus in sedimentary rocks, that of SiO_2/Al_2O_3 as a marker of the presence of quartz in relation to clay minerals and feldspar (Cullers, 2000). Ver Straeten et al. (2011) indicated a Si/Al ratio above 5 as a tracer for sand-dominated clastic supply. The analysed samples show SiO_2/Al_2O_3 ratios which vary over a wide range from 1.9 to 11.1 at TPP and from 2.5 to 6.9 in MS (Figs. 12 and 13). This suggests that the amount of quartz varies relative to feldspar or Al-rich clay minerals.

As stressed in the introductory geochemical characteristics, marked differences exist in siliciclastic input between the Thai sections. At the oceanic MS ridge, this delivery, probably mainly aeolian and/or diluted turbidite, was certainly strongly overwhelmed by carbonate deposition, with the strongest impact of clay input in the inter-KW interval (cf. data from South China in Whalen et al., 2015). However, coarse-grain tracers (Zr/Al and Si/Al) indicate a somewhat inconsistent secular pattern in the Late Frasnian, likely due to varying volcaniclastic admixture and/or sorting/recycling phenomena (Figs. 12 and 17; see below). They certainly indicate several episodes of quartz sand input with abundant heavy minerals (zircon, rutile, ?ilmenite, ?titanite), particularly in the Upper Frasnian interval. The Zr/Rb ratio from other indices (not shown in figures) is highlighted, because these immobile constituents are preferentially enriched in terms of material characterized by either coarser grain-size (Zr) or finer detrital fraction (Rb); this proxy variation also indicates episodically increased coarse-fraction abundance. On average, lower levels of the proxy values are observed in the Famennian slice, constituting evidence of a more stabilized carbonate-dominated depositional regime. Therefore, the terrigenous admixture exhibits a generally decreasing trend upward the succession, even if it fluctuates irregularly in the Frasnian portion, likely forced by eustatic fluctuations (see Fig. 10). The secular changes recorded geochemically in the siliciclastic phase were everywhere largely governed by tectonic and/or climatic factors in the source areas (see more data in Section 8).

At Thong Pha Phum, the entire elemental signature is influenced by fluvial-dominated(?) siliciclastic input to the somewhat starved outer-shelf domain, manifested in extensive correlative links (see Appendix

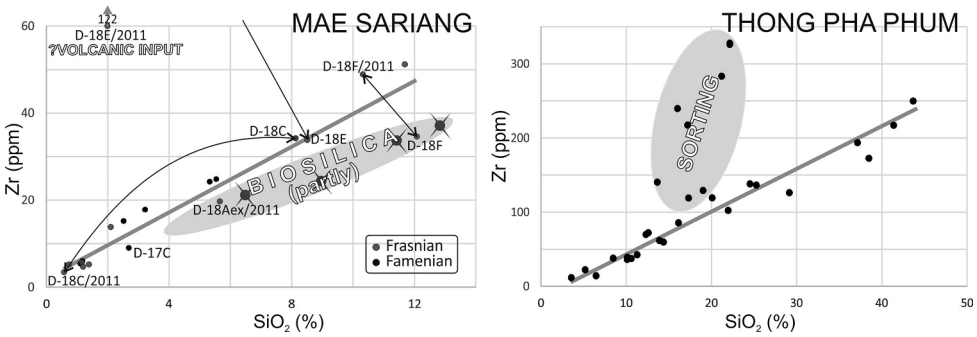

Fig. 17. Cross-plot of SiO_2 and Zr used to differentiate between silica of detrital origin (positive correlation; background trend shown) and biogenic production (negative correlation; see, e.g., Dong et al., 2018). Note the dissimilarity between the two Thai sections, with sedimentary processes recorded only in TPP as opposed to a biosilica admixture in MS. Additional radical differences between the 2009 and 2011 results from Mae Sariang are shown by arrows for three cases (D18-C, -E, -F), suggesting abrupt lateral changes and/or successive sampling of slightly different stratigraphic horizons in the highly condensed oceanic succession.

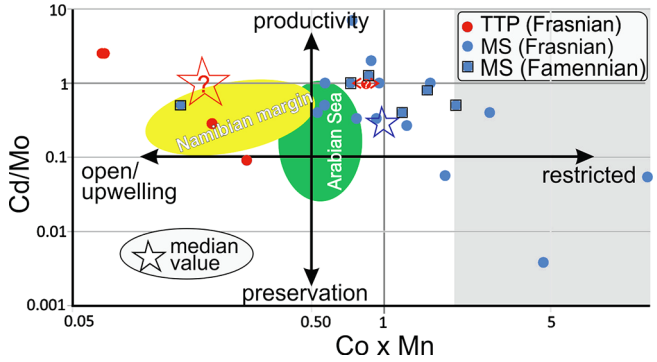

Fig. 18. Co × Mn versus Cd/Mo proxies applied to the Thai successions, after Sweere et al. (2016, Figs. 6, 7), to the distinction between open/upwelling and restricted marine settings, along with a comparison to Recent Namibian (TTP) and Arabian (MS) settings. Only some Frasnian samples are presented for the TPP locality due to mostly insufficient contents of Mo and Cd (below detection levels) in the Famennian slice.

1). The clay admixture is clearly enriched in the middle portion of the succession, whereas the content of the coarse-grained fraction exhibits high but variable abundances in the lower segment (also positively correlated with, e.g., Zr/Rb ratios), Therefore, synsedimentary tectonic and, perhaps, climatic factors (see below) can be assumed in addition to eustatic control (Fig. 10). Recycling phenomena, guided by a Th-Zr/Sc proxy and a $15Al_2O_3 - Zr - 300 \times TiO_2$ plot (Fig. 14; McLennan et al., 1993), are also evidently recorded in the Frasnian interval.

7.3. Weathering and climate changes in sediment source areas

The high-resolution oxygen isotope signature, derived from monogeneric conodont apatite, evidences a subtropical surface water cooling of ~3 °C in the LKW and ~6 °C in the UKW event (Huang et al., 2018a; see also Song et al., 2017). On the other hand, from pedogenic data Retallack and Huang (2011) postulated CO_2/greenhouse spikes for the both KW events, recognizable rather as the pre-KW episodes in the oceanic paleotemperature curve (Fig. 1). Concomitant pulses of enhanced continental weathering are implied from osmium-isotope trends (Percival et al., 2019). Thus, in the crucial climate context of the F-F biocrisis, four proxies [Al/Ti, K/Th (the ratio is reversed for illustrative reasons in Figs. 12 and 13), as well as not illustrated here Ga/Rb and K/Rb] are selected among proposed elemental ratios. The tracers are interpreted in the recent literature to be climate-driven owing to different element behavior in humid vs. arid weathering regimes in the sediment source areas (see Ratcliffe et al., 2010; Kiipli et al., 2012; Lo et al., 2017). In particular, as shown by Lash (2017) for the F-F passage of New York, K/Th ratio is a potential key for interpretation of climate moisture and warmth, because K is selectively mobilized from clay and feldspars under hot and moist conditions, conversely to relatively insoluble Th. Considering Al and Ti, overall immobile elements, their solubility changes with pH and therefore is related with the intensity of chemical weathering (Kiipli et al., 2012). The selective use of only clay fraction is preferred for this proxy, but the elements are strictly correlated in the Thai sections (r = 0.98 at MS and 0.78 at TPP), and the bulk sample results are introductorily tested in the climate context (i.e., jointly with Ti-bearing detritus).

Only the Al/Ti trend suggests slightly variable weathering conditions recorded in the delivered siliciclastic fraction in the limestones of MS, with a clearly identifiable cooling interval in the early UKW timespan. Two further proxy values (K/Th, Ga/Rb) are more stable, with some excursions indicating cooler setting, more distinctively expressed in the broad F-F transition. Alleged K/Rb fingerprint suggests the rapidly increasing but fluctuating intensity of weathering processes in a warm/humid regime restricted to the F-F boundary interval.

In terms of climatic proxies at TPP, Al/Ti values again reveal highly unstable regimes, with an alleged cool episode prior to the F-F boundary. The K/Th trend is much steadier, but some shifts suggestive of relatively humid interludes are recorded at with the LKW CIE and inter-KW time spans. K/Rb ratios unexpectedly point to a cooling interval in the inter-KW interval. To summarize, the climatic perturbations appear to be highly obscured in the multi-proxy analysis of the both Thai basins, although the most disturbed weathering conditions are partly evidenced in the UKW interval, at least at MS.

7.4. Redox conditions and bioproductivity

As already noted, several chalco- and siderophile constituents are

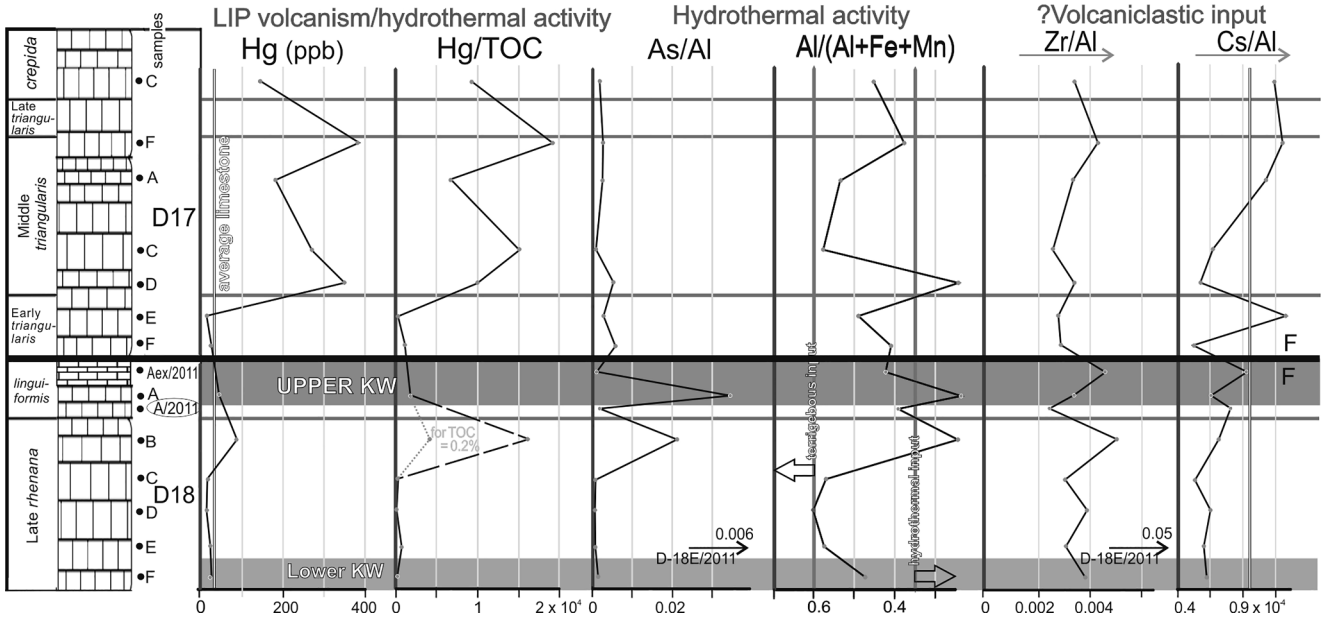

Fig. 19. Secular trends of selected geochemical proxies for volcanic and hydrothermal activity in the Mae Sariang section (see also Fig. 12). Note anomalous Zr/Al and As/Al ratios for the supplementary sample D18-E/2011 (see Fig. 17), which are not confirmed by Hg and Cs abundances (see Appendix 2), as well as mostly increased Hg and Hg/TOC values in the Famennian slice, paired with a modest Hg enrichment in the inter-KW interval, biased by the extreme TOC impoverishment.

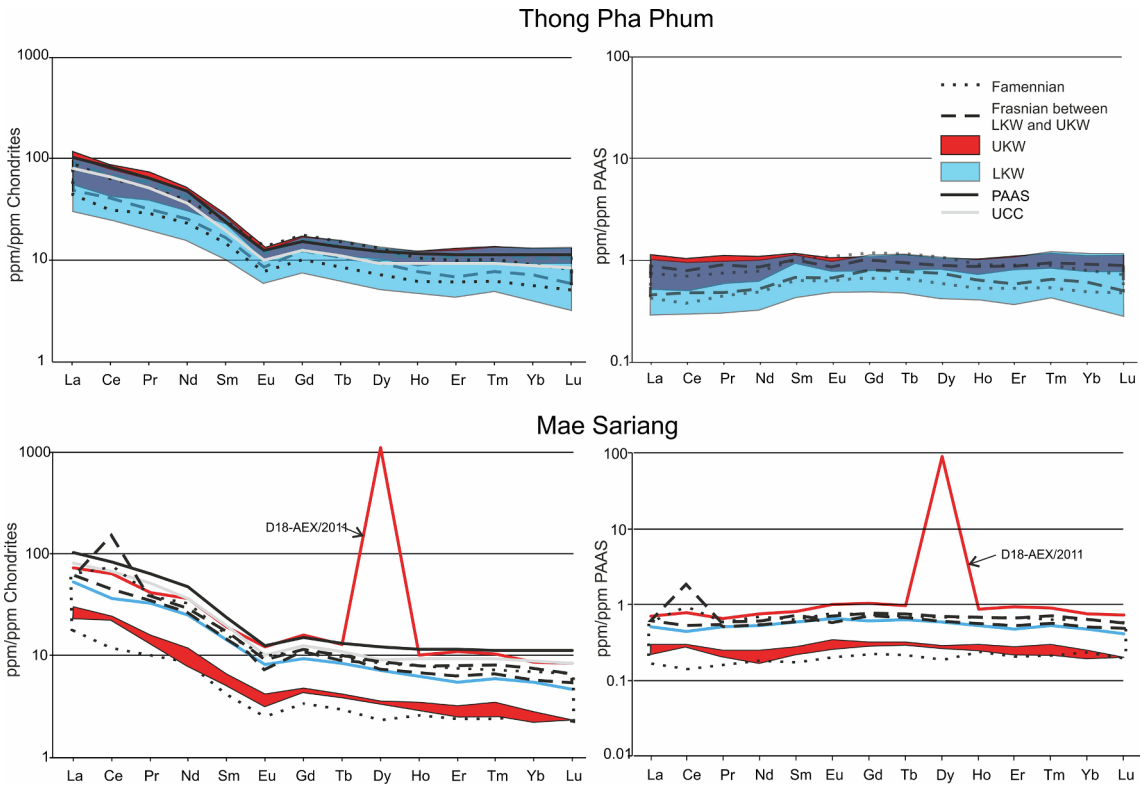

Fig. 20. Carbonate-corrected REE patterns from the Thong Pha Phum and Mae Sariang successions. PAAS, UCC, and chondritic normalization values are from McLennan (2001). Note the unusual Dy geochemical signature in the sample MS-D18-Aex/2011 from fungal-mediated(?) hard grounds at the top of the Frasnian (see Figs. 4 and 5).

marked by average excess (EFs more than 3; see Fig. 11), and therefore prove a significant authigenic and/or biogenic phase contribution in these sediments. As a result of further tests of potential productivity or redox-sensitive proxies (see reviews in Brumsack, 2006; Tribovillard et al., 2006; Harris et al., 2018; Ocubalidet et al., 2018; for a more refined approach, see Dong et al., 2018), elements not correlated with Si (quartz) and/or Al (clay) contents were identified (see Appendix 1). This preference is easily assessed in the case of the MS section, where such refuting links are generally absent for Mo (r = −0.05 with Al), Co (−0.05), Cu (−0.49), Ni (0.33), and V (0.38), whereas P and Zn are modestly correlated with clay content (r = 0.62 and 0.51, respectively). Only Ba and U values are more strongly controlled by the aluminosilicate fraction (0.79 and 0.76, respectively), whereas Cr concentrations are below the detection level (except in one sample). TOC content and $\delta^{13}C$ values are not correlated with the clay admixture in either section.

The highest values of the temporal variations of Al-normalized redox-sensitive trace metals, including the most reliable, Mo, are observed in the middle part of the MS succession (Fig. 15). In particular, the notable authigenic enrichment of Mo (21 ppm) in sample D18-A (confirmed by the anomalous sample D18-E/2011; see Fig. 17) points to a severe oxygen-deficient episode in the UKW interval (*sensu stricto*), as concluded by Savage (2013). Other proxies (U/Th, V/Al, Ni/Co) show fluctuating values in a broader interval around the F-F boundary. However, a closer determination of potentially deleterious oxygen depletion reached with the use of thresholds proposed for several proxies appears to be unreliable. As usual, with the exception of V/(V + Ni), these data point to, at most, weakly reducing conditions (especially Ni/Co ratios; see similar discrepancies in Racka et al., 2010; Ocubalidet et al., 2018, and references therein). For both Mo-rich upper Frasnian samples, the contrasted abundances of Mo and U imply an excess of molybdenum resulting from the cyclicity of manganese or iron oxyhydroxides on the surface of the sediment or within the water column, as argued by Riboulleau et al. (2018; see also Algeo and Tribovillard, 2009). Irrespective of a wide range of potential biases, the analyzed sediments certainly represent mainly oxic depositional settings.

The productivity tracers show a broadly similar secular trend at Mae Sariang, with positive excursions consistently grouped in the UKW level (Fig. 15), even if this is partly connected with a terrigenous and/or hydrothermally-related supply of nutrients (e.g., a model by Algeo et al., 1995; see below). Furthermore, this chemostratigraphical pattern agrees with a positive $\delta^{13}C$ excursion (Figs. 8 and 9) and, partly, with increased TOC values.

At the Thong Pha Phum site, assessment of both environmental factors is significantly limited due to the extensive influence on the potential tracers exerted by the siliciclastic fraction, as also clearly proven by their common relative depletion (see Fig. 16; Appendix 1). All redox-sensitive constituents are positively correlated with Si and Al; however, U shows the markedly weakest association (r = 0.51 with Al). In terms of potential productivity tracers, only Cu (−0.20), and, to some extent, Zn (0.59) and P (0.54) are trustworthy elements.

Taken together, the mostly authigenic U/Th proxy (between 0.3 and 1.4; Fig. 11; but also e.g., V/Cr values below 2.2) and Mo concentrations below the detection level in 18 of 20 samples (maximally 1.1 ppm in the inter-KW slice) argue for oxic conditions in the deep-shelf domain. More complex relationships exist between elemental proxies of primary production, TOC and $\delta^{13}C$ time series. The higher values of the two latter indicators are largely correlated with the two KW CIE intervals. Conversely, both Cu values and Al-normalized Cu, Zn, and P tracers suggest, to varying degrees, phytoplankton acmes grouped in the inter-KW timespan, and only in the LKW CIE interval (especially P/Al ratios).

In brief, the multi-proxy analysis in the Thai sections provide only partial support for the usually accepted global scenarios, connecting the organic-enriched KW horizons (Fig. 1) with extensive oceanic eutrophication and progressive anoxia (see Joachimski and Buggisch, 2002; Racki et al., 2002; Bond et al., 2004; Racki, 2005; Whalen et al.,

2015; compare Carmichael et al., 2019). This correlation is again more clearly evidenced at MS. In fact, the secular pattern at TPP contradicts any oxygen deficiency in the key KW Crisis period, suggesting instead some land-derived eutrophication pulses clearly limited to the Late Frasnian.

In a paleoenvironmental context, differentiation of the Thai successions is additionally evidenced by open marine/upwelling vs. restricted marine proxies, as recently proposed on a reliable actualistic basis by Sweere et al. (2016) for the main factors governing organic matter enrichments. Despite some limitations, especially at the TPP site [overall very low TOC (median value 0.1%; max. 0.55%) and key trace-metal abundances], several implications are rather obvious, in both temporal and geographical contexts (Fig. 18). In particular, far more variable influences on productivity-controlled accumulation are notable in both sections during the Frasnian age. A startling tendency toward a restriction of circulation in the pelagic MS locality is particularly puzzling (likely due to synsedimentary tectonics?).

There is a great deal of evidence for a worldwide biosiliceous acme (silicisponges, radiolarians) in the KW interval, thought to be a biotic response to the biocalcification crisis and an overall carbonate factory collapse (see summaries in Racki, 1999, 2005). According to microfacies data, radiolarians occur only in the Frasnian slice of the Mae Sariang section (Fig. 4; cf. Königshof et al., 2012). Geochemical testing, guided by a SiO_2 vs. Zr cross-plot (following Dong et al., 2018 and Harris et al., 2018; Fig. 17), exhibited positively covarying ratios for exclusively terrestrially-derived silica at TPP, with clear sorting/recycling processes (see also Fig. 14A). More complex Si sources are revealed in the latest Frasnian at MS, where a major detrital background trend was supplemented by biogenic, and likely volcanic, processes (Fig. 17). In particular, increased oceanic radiolarian productivity in the Paleotethys is shown, in partial agreement with microfacies data (especially sample D18-F, with an excess of silica relative to zircon of ca. 30%). However, a clearly biased abundance signature, as an effect of the calcitization process of biogenic opal in the carbonate matrix, is noteworthy (see, e.g., the F-F data in Racki et al., 2002). Thus, the underlined biosiliceous KW episode may be assumed for the Mae Sariang locality only, in the form of rare radiolarian productivity pulses, recorded similarly to those for certain Laurussian carbonate shelf successions (e.g., Hladil et al., 1991; see review in Racki, 1999).

7.5. Volcanic/hydrothermal activity

Several elemental bits of data are considered to reflect volcanic signals (e.g., Suzuki et al., 1998; Sageman and Lyons, 2003; Grasby et al., 2015, 2019), which include those in the context of concurrent F-F tectono-magmatic activation (see Racki, 1998; Racki et al., 2002; Yudina et al., 2002; Averbuch et al., 2005; Pujol et al., 2006; Weiner et al., 2017). In particular, the composition of wind-blown dust may be strongly influenced by eruptive paroxysms, as reflected by high Zr and Ti abundance levels in a fine-grained volcaniclastic admixture. However, alternative interpretations have been conclusively presented for these ratios, including the aspects of climate, sediment, and provenance (e.g., Sageman and Lyons, 2003; see Figs. 12 and 13 for Al/Ti trends). Excessive accumulations of, e.g., As, Co, Cu, Mo, Ni, Pb, Sb, and Zn, have been observed in recent and ancient sediments from areas of hydrothermal activity (Gurvich, 2006; Nath et al., 2008).

As oceanic hydrothermal deposits are characterized by Al/(Al + Fe + Mn) values less than 0.35 and Fe/Ti values higher than 20 (Boström, 1983), these elemental relationships were employed as tracers of hydrothermal supply. In addition, two other Al-normalized elements were tested in this study:

- arsenic, authigenic in the Thai sections (correlation with Al: r = −0.02 and ca. −0.6 at MS and TPP, respectively), for tracing of hydrothermal mineralization processes due to the enrichment of this element in hydrothermal plumes and its incorporation into polymetallic deposits (Nath et al., 2008; Breuer and Pichler, 2013; ?also in LIP-related emissions, Grasby et al., 2015);
- cesium, as a marker of volcanic ash contribution, due to its relationship to the proportion of illite/smectite in the clay fraction (Ratcliffe et al., 2010).

Thus defined, the record of magmatic processes is scantily represented at TPP (Fig. 16), where Zr and Ti (and also Fe?) concentrations constitute an obvious record of sorted/recycled terrigenous input (see below). The crucial tracers are depleted in the succession (note the negative EFs in Fig. 10). In fact, whereas high Al-Fe-Mn proxy values contradict the significant influence of hydrothermal processes, less trustworthy Fe/Ti and As/Al variations suggest that the plume delivery may have occurred exclusively in the late LKW CIE interval.

The elemental signature of hydrovolcanic processes is more significantly expressed at the MS site (Fig. 16), as previously suggested by Savage (2013, 2019) for the brownish level D18-AEx. Despite largely terrigenous-related Fe contents (r = 0.55 for correlation with Al), the mostly authigenically driven As/Al and Al-Mn-Fe proxies (see highly positive EFs in Fig. 10) collectively point to an increased hydrothermal signature in the broad F-F transition. This activity (confirmed as well by high Fe/Ti ratios) probably contributed as well to episodic oxygen depletion and eutrophication at that time. Noteworthy in this context is that As is generally positively correlated with Co, V, and Pb (r = 0.58, 0.65, and 0.81, respectively), but not with Fe and Mn (0.04 and −0.15, respectively). Also noteworthy is the similar geochemical behavior of another less abundant hydrothermal tracer, antimony, which co-varies with As (r = 0.94; see Appendix 1). This differentiation of elements, including As, Cu, Co, Pb, Sb, and Fe, probably reflects different stages of hydrothermal mineral formation and sedimentation with increasing distance from hydrothermal vents (Gurvich, 2006).

Winter (2015) recently reported numerous very thin metabentonites in Central European successions which constitute a record of intensification of alkaline volcanism during the KW interval. On the other hand, refined insights in mercury chemostratigraphy over the past few years have finally resulted in the assessment of a consistent worldwide tracer for volcanic paroxysms (via Hg-rich gaseous expulsions in the stratosphere), particularly in large igneous provinces (LIPs). This causal link has been evidenced by anomalous Hg enrichments in the levels of four mass extinctions and a number of subordinate biotic crises (Clapham and Renne, 2019; Grasby et al., 2019). In particular, Racki et al. (2018b) reported multiple Hg spikes in F-F boundary beds in Morocco, Germany, and northern Russia, with the most distinct and likely LIP-related mercury signal just below the F-F boundary.

Within the conceptual framework of these current results, the Thai sections again present somewhat contrasting signatures. At TPP, Hg concentrations in the studied samples are below the detection level in ICP MS measures (10 ppb; below 30 ppb in 7 samples analyzed by AAS method; Appendix 2). On the other hand, modest Hg excess is observed in the Famennian portion at MS (but not in the key sample D18-Aex), and is even more than doubled in high-resolution AAS measurements (140 vs. 382.5 ppb in D16-F; Fig. 19). Following normalization to TOC, two Hg spikes can be observed in the Middle *triangularis* Zone, and also in the inter-KW interval (D18-B), but oversized due to extremely impoverished organic matter (0.05%) in the sample. It has been argued by Grasby et al. (2019) that normalization of Hg against TOC is biased in the case of biased, very low values of TOC contents (< 0.2%). Furthermore, the sample D18-B shows an augmented hydrothermal signature (e.g., a maximal As value of 59.2 ppm); therefore only the regional extent of this Hg signal is probable (see Percival et al., 2018; Jones et al., 2018).

Consequently, correlation of Hg-enriched levels with the assumed Sextans and early Scorpius eruptive events *sensu* Winter (2015; Fig. 1) is extremely hypothetical, even if it can be referred to the assumed scenario of a pulsatory pattern of worldwide tectono-magmatic activation and LIP paroxysms within the broadly defined KW Crisis period (Racki,

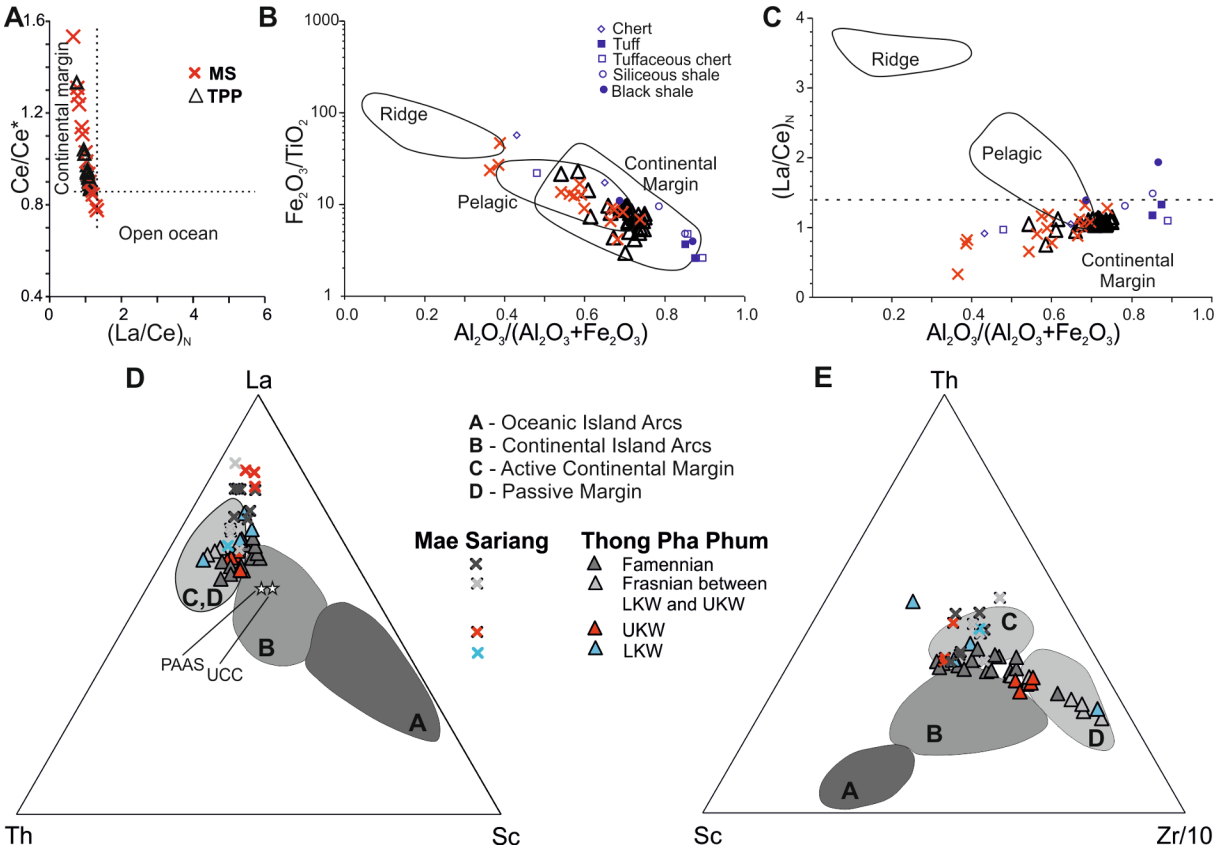

Fig. 21. (A–C) Plots of $(La/Ce)_N$ vs Ce/Ce*, $Al_2O_3/(Al_2O_3 + Fe_2O_3)$ versus Fe_2O_3/TiO_2, and $(La/Ce)_N$ showing data for the Thai successions (this study) and the Devonian siliceous succession in the Chiang Dao area of northern Thailand for comparison (blue marks; Hara et al., 2010). The fields of ridge, pelagic, and continental margin are from Murray (1994) and Zhang et al. (2017). (C and D) Ternary plots of La–Th–Sc and Th–Sc–Zr/10 (Bhatia and Crook, 1986) for the differentiation of tectonic settings of the TPP and MS successions. PAAS and UCC values from McLennan (2001; Table 2).

1998; Averbuch et al., 2005; Riquier et al., 2006; Racki et al., 2018b; see also Percival et al., 2019). In fact, anomalous metal loading from LIP eruptions, which also includes As, Cu, Pb, and Cd (all of which are notably enriched in sample D18-E/2011; Fig. 17 and Appendix 2), is shown for the end-Permian eruption of the Siberian Traps (Grasby et al., 2015, 2019). Thus, the missing signature of anomalously Hg-rich

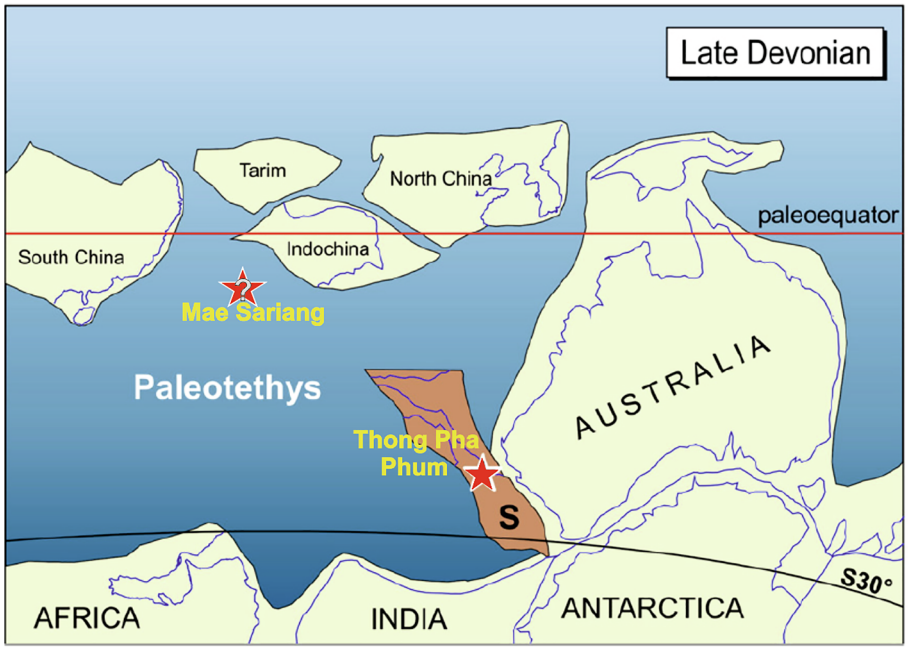

Fig. 22. Late Devonian paleogeographic reconstruction of the eastern Gondwanan/Chinese domain (based on Dopieralska et al., 2012, Fig. 5; cf. Fig. 8.4 in Torsvik and Cocks, 2017) to show the differing geotectonic positions of the two studied Thai localities (asterisks).

horizons, typically very thin in other more stratigraphically extended sections (see Racki et al., 2018b), can be explained by the erratic record of brief events in the very condensed deposits. Moreover, dominantly oxic and likely oligotrophic conditions were unfavorable for the preservation of Hg overloading (see Bergquist, 2017; Percival et al., 2018; Jones et al., 2018; Grasby et al., 2019).

On the other hand, in this uncertain climatic setting (see above), tectonic pulses, remodeling sediment source terrains, are the most probable factor recorded in the peaks of distinctly increased coarse-grained terrigenous input, conspicuously limited to the Frasnian part of both Thai successions. Notably, Torsvik and Cocks (2017, p. 141, Fig. 8.3) noted an example of tectono-magmatic activation in south-eastern Gondwana in the Late Devonian, involving the intrusion of kimberlites between 382 and 367 Ma, and sourced by the Pacific mantle plume (see also episodic contractional deformations of Tasmanides in Rosenbaum, 2018).

8. Provenance and geotectonic setting (Pisarzowska)

As shown above, most of the isotopic and trace metal geochemical proxies point to distinct paleoenvironmental differentiation between the two Thai successions. The limestones, deposited near continents, were influenced geochemically upon terrigenous material, therefore the REE abundances for the limestones show a distinct positive correlation with Al_2O_3, SiO_2 and TiO_2 (Zhang et al., 2017). The geochemistry of open ocean limestones is more dependent upon the flux of hydrothermal Fe–Mn oxyhydroxides whereas their REEs and trace elements are positively correlated with MnO (Zhang et al., 2017). Additionally, an average composition of open oceanic limestones is characterized by lowest Al_2O_3, Fe_2O_3 and most strongly negative Ce anomalies [calculated as $Ce/Ce^* = 2Ce_N/(La_N + Pr_N)$] and, simultaneously, by strongly positive La anomalies [$(La/Ce)_N$]. The ΣREEs for the TPP limestones are positively correlated distinctly with TiO_2, SiO_2, and Al_2O_3 ($r = 0.92$; $r = 0.91$; $r = 0.69$, respectively) and negatively correlated with MnO ($r = -0.11$). The ΣREEs for the MS (except the anomalously REE-enriched Frasnian samples D-18B and D-18Aex/2011) are also positively correlated with Al_2O_3, SiO_2, TiO_2, and MnO ($r = 0.69$; $r = 0.66$; $r = 0.62$; $r = 0.25$, respectively). Ce/Ce* ratio at studied sections are generally below 1.0, while La_N/Ce_N are above 1.0 (Fig. 21). The observed variations indicate the influence of detrital siliciclastic fraction on the REE at TPP, whereas the REE pattern at MS is governed by multiple factors, such as detrital and hydrothermal input.

Because the differences in trace elements and REE content between the analyzed Thai sections might result mainly from the volume of terrigenous materials in the carbonate rocks (see Section 7.1; Figs. 12–14, 17, 20, 21), the analyzed samples were compared with the UCC and PAAS in the La-Th-Sc diagram (Bhatia and Crook, 1986; Fig. 21). The provenance ratios correspond with the values for felsic (feldspar- and silica-rich) rocks (Cullers, 2000).

The influence of the tectonic environments of the basins on limestone geochemistry enables the development of proxies for the differentiation of depositional regimes (Zhang et al., 2017). The geochemical composition of the studied limestones suggest mainly continental margin and subsequently continental island arc settings (Fig. 21). A systematic increase in the magnitude of Ce anomalies and simultaneous decrease in the magnitude of La anomaly depending on proximity of the basin to a continental plate margin (Hara et al., 2010; Zhang et al. 2017; Fig. 21). According to Bhatia (1985), terrigenous material of the active continental margins and continental island arc is derived from felsic-volcanic or granite-gneissic rocks, that of the passive margin predominantly from older, continental sedimentary-metasedimentary rocks (compare other proxies in Fig. 13). During the opening of the Paleotethys the felsic tuffs and tuffaceous cherts were deposited in the Middle-Late Devonian siliceous succession in the Chiang Dao area, northern Thailand (Hara et al., 2010). Dopieralska et al. (2012) suggested a passive margin continental setting of TPP and input of non-radiogenic Nd from eroded Paleoproterozoic and Neoarchean rocks in the surrounding continental area (see Fig. 22). This hypothesis can be supported by the influence of detrital siliciclastic fraction on the trace elements and the REE at TPP (Fig. 21), typical of continental margin settings (Bhatia and Crook, 1986; Zhang et al., 2017).

9. Final remarks and conclusions

1. The two studied Thai limestone sections of the F-F transition differ significantly in terms of depositional and geochemical signature, which can be explained only in part by the more marly character of the Thong Pha Phum succession. The highly condensed (paired partly with microbial biosedimentary activitiy), monotonous Mae Sariang pelagic limestone succession generally corresponds to the worldwide F-F event pattern (Fig. 1). Nevertheless, only briefly enduring anoxic conditions are identifiable in the key crisis timespan of the succession, which is devoid of dark, organic-rich intercalations (Savage, 2013).
2. In the case of Thong Pha Phum, two specific characteristics are especially notable for both KW events marked by regressive tendencies (Fig. 10):
   - the $\delta^{13}C$ positive excursion, determining the Upper KW level, is peculiarly two-staged, with a distinctly lower amplitude (below 1.5‰) and a highstand plateau prolonged to the Late *triangularis* Zone (Savage et al., 2006);
   - elemental proxies and fossil-rich microfacies indicate exclusively oxic and probably oligotrophic conditions during the $\delta^{13}C$ excursion of UKW and at least in the upper part of LKW.
3. In the microfacies record, the worldwide biosiliceous acme in the terminal Frasnian (Racki, 1999) is identifiable exclusively in radiolarian productivity bursts in the Mae Sariang oceanic succession (Fig. 17). More consistent pattern in the Thai sections probably represents the UKW-related demise of calcareous plankton, i.e., tentaculitid and entomozoacean ostracod associations (Figs. 4 and 6; see Gereke and Schindler, 2012; Huang et al., 2018; Komatsu et al., 2019; Ma et al., 2016). With respect to conodont biofacies, the abrupt worldwide increase of *Icriodus* abundance in the basal Famennian (Sandberg et al., 1988; Huang et al., 2018b), is obscured in both of the studied successions (see Savage et al., 2006; Savage, 2019).
4. The exposed biogeochemical, environmental, and provenance-related variations confirm the contrasting paleogeographic locations of the studied successions, as indicated by the Nd isotope composition of Late Devonian seawater in western Thailand (Dopieralska et al., 2012; Fig. 22). The distinctiveness of the TPP section clearly indicates its affinity with Western Australian shelf successions, characterized by the well-known “atypical” record of the F-F biocrisis (Fig. 9).
5. Geochemical proxies of climate, despite their successful application to other Devonian successions, provide an inconsistent picture of the intra-KW climatic perturbations recorded in both paleogeographic regions (see Figs. 12 and 13). The highlighted global cooling during the UKW (Huang et al., 2018a) is therefore uncertainly identified in this part of Asiatic-Australian domain.
6. In reference to the recently propagated tectono-volcanic scenario, the Thai sites point primarily to mostly tectonically driven (and/or regressive; Figs. 10 and 17) episodes of distinctly increased and relatively coarser-grained terrigenous delivery (even if not exactly in the KW intervals *sensu stricto*, see also Whalen et al., 2015). Coeval magmatic activity (Torsvik and Cocks, 2017; Racki et al., 2018b; also Zhang et al., 2019) appears to be geochemically recorded only as mostly terminal Frasnian hydrothermal signals in the Paleotethyan domain.
7. From the perspective of provenance (Fig. 21), the Paleotethyan MS succession corresponds to a continental margin where terrigenous delivery was sourced from felsic-volcanic or granite-gneissic rocks.

In the case of the TPP section, a passive continental margin, a partly active margin, and the continental island arc are recorded in the detritus, predominantly derived from older continental sedimentary-metasedimentary terrains. Therefore, the Western Australian geotectonic assignment of TPP corresponds to the variable, partly recycled material supplied abundantly to the "Sibumasu depocenter" from adjoining granite-dominated Archean cratons (Fig. 22).

Declaration of Competing Interest

The authors declare that they have no known competing financial interests or personal relationships that could have appeared to influence the work reported in this paper.

Acknowledgements

We sincerely thank Norman Savage for initiation of the F-F boundary study in Thailand, providing samples and geochemical data, and the kind support for this study. We gratefully acknowledge the three journal reviewers, Professor Clive Burrett and two anonymous reviewers, for their thorough and insightful reviews and valuable suggestions to improve the quality of your manuscript in the acknowledgements as well as Professor Khin Zaw for handling the manuscript and editorial input. We also gratefully acknowledge Apsorn Sardsud for help in field works in 2010-2012 and Justyna Smolarek-Łach for TOC measurments. This research was funded in part by the National Science Centre – Poland (MAESTRO grant 2013/08/A/ST10/00717 to G.R.).

Appendix A. Supplementary material

Supplementary data to this article can be found online at https://doi.org/10.1016/j.jaesx.2019.100010.

References

Algeo, T.J., Berner, R.A., Maynard, J.B., Scheckler, S.E., 1995. Late Devonian oceanic anoxic events and biotic crises: "rooted" in the evolution of vascular land plants? GSA Today 5 (45), 64–66.
Algeo, T.J., Tribovillard, N., 2009. Environmental analysis of paleoceanographic systems based on molybdenum-uranium covariation. Chem. Geol. 268, 211–225.
Arthur, M.A., Dean, W.E., 1991. A holistic geochemical approach to cyclomania; examples from Cretaceous pelagic limestone sequences. In: Einsele, G., Ricken, W., Seilacher, A. (Eds.), Cycles and Events in Stratigraphy. Springer Verlag, Berlin, pp. 126–166.
Averbuch, O., Tribovillard, N., Devleeschouwer, X., Riquier, L., Mistiaen, B., van Vliet-Lanoe, B., 2005. Mountain building-enhanced continental weathering and organic carbon burial as major causes for climatic cooling at the Frasnian-Famennian boundary (ca 376 Ma BP). Terra Nova 17, 25–34.
Barber, A.J., Ridd, M.F., Crow, M.J., 2011. The origin, movement and assembly of the pre-Tertiary tectonic units of Thailand. In: Ridd, M.F., Barber, A.J., Crow, M.J. (Eds.), The Geology of Thailand. Geological Society, London, pp. 507–537.
Barr, S.M., Macdonald, A.S., 1991. Toward a Late Paleozoic-Early Mesozoic tectonic model for Thailand. J. Thailand Geosci. 1, 11–22.
Baum, F., Braun, E.V., Hess, A., Koch, K.E., 1982. Geologic Map of Northern Thailand, Chiang Mai Sheet. Federal Institute for Geosciences and Natural Resources, Germany 250 000.
Becker, R.T., Gradstein, F.M., Hammer, O., 2012. The Devonian Period. In: In: Gradstein, F.M. (Ed.), The Geologic Time Scale 2012 v. 2. Amsterdam, Elsevier, pp. 559–601.
Bergquist, A.B., 2017. Mercury, volcanism, and mass extinctions. Proc. Natl. Acad. Sci. U. S. A. 114, 8675–8677.
Bhatia, M.R., 1985. Composition and classification of Paleozoic flysch mudrocks of eastern Australia: implications in provenance and tectonic setting interpretation. Sediment. Geol. 41, 249–268.
Bhatia, M.R., Crook, K.A.W., 1986. Trace element characteristics of graywackes and tectonic setting discrimination of sedimentary basins. Contr. Min. Petrol. 92, 181–193.
Böhm, F., Ebli, O., Krystyn, L., Lobitzer, H., Rakus, M., Siblik, M., 1999. Fauna, stratigraphy and depositional environment of the Hettangian-Sinemurian (Early Jurassic) of Adnet (Salzburg, Austria). Abh. Geol. Bund. Wien 56 (2), 143–271.
Boström, K., 1983. Genesis of ferromanganese deposits – diagnostic criteria for recent and old deposits. In: Rona, P.A., Boström, K., Laubier, L., Smith, K.L. (Eds.), Hydrothermal Processes at Seafoor Spreading Centers. Plenum Press, New York, pp. 473–489.
Brand, U., Tazawa, J., Sano, H., Azmy, K., Lee, X., 2009. Is mid-late Paleozoic ocean-water chemistry coupled with epeiric seawater isotope records? Geology 237, 823–826.
Breuer, C., Pichler, T., 2013. Arsenic in marine hydrothermal fluids. Chem. Geol. 348, 2–14.
Brumsack, H.J., 2006. The trace metal content of recent organic carbon – rich sediments: implications for Cretaceous black shale formation. Palaeogeogr. Palaeoclimatol. Palaeoecol. 232, 344–361.
Buggisch, W., Joachimski, M.M., 2006. Carbon isotope stratigraphy of the Devonian of Central and Southern Europe. Palaeogeogr. Palaeoclimatol. Palaeoecol. 240, 68–88.
Burkhalter, R.M., 1995. Ooidal ironstones and ferruginous microbialites: origin and relation to sequence stratigraphy (Aalenian and Bajocian, Swiss Jura Mountains). Sedimentology 42, 57–74.
Burrett, C.F., 1974. Plate tectonics and the fusion of Asia. Earth Planet. Sci. Lett. 21, 181–189.
Calvert, S.E., Pedersen, T.F., 2007. Elemental proxies for palaeoclimatic and palaeoceanographic variability in marine sediments: interpretation and application. Dev. Mar. Geol. 1, 567–644.
Carmichael, S.K., Waters, J.A., Königshof, P., Suttner, T.J., Kido, E., 2019. Paleogeography and paleoenvironments of the Late Devonian Kellwasser Event: a review of its sedimentological and geochemical expression. Glob. Planet. Change, 102984. https://doi.org/10.1016/j.gloplacha.2019.102984.
Chang, J.Q., Zhiqiang Bai, Z.Q., Sun, Y.L., Peng, Y.B., Qin, S.J., Shen, B., 2019. High resolution bio- and chemostratigraphic framework at the Frasnian-Famennian boundary: implications for regional stratigraphic correlation between different sedimentary facies in South China. Palaeogeogr. Palaeoclimatol. Palaeoecol. 531A (108299), 1–14.
Chen, D., Qing, H., Li, R., 2005. The Late Devonian Frasnian-Famennian (F/F) biotic crisis: insights from $\delta^{13}C_{carb}$, $\delta^{13}C_{org}$ and $^{87}Sr/^{86}Sr$ isotopic systems. Earth Planet. Sci. Lett. 235, 151–166.
Chen, D., Wang, J., Racki, G., Li, H., Wang, C., Ma, X., Whalen, M.T., 2013. Large sulphur isotopic perturbations and oceanic changes during the Frasnian-Famennian transition of the Late Devonian. J. Geol. Soc. 170, 465–476.
Christ, N., Immenhauser, A., Wood, R.A., Darwich, K., Niedermayr, A., 2015. Petrography and environmental controls on the formation of Phanerozoic marine carbonate hardgrounds. Earth-Sci. Rev. 151, 176–226.
Clapham, M.E., Renne, P.R., 2019. Flood basalts and mass extinctions. Annu. Rev Earth Planet. Sc. 47, 275–303.
Craigie, N., 2018. Principles of Elemental Chemostratigraphy. A Practical User Guide. Springer, Cham, pp. 189.
Crasquin, S., Horne, D.J., 2018. The palaeopsychrosphere in the Devonian. Lethaia 51, 547–563.
Cullers, R.L., 2000. The geochemistry of shales, siltstones and sandstones of Pennsylvian-Permian age, Colorado, USA: implications for provenance and metamorphic studies. Lithos 51, 181–203.
Dera, G., Prunier, J., Smith, P.L., Haggart, J.W., Popov, E., Guzhov, A., Rogov, M., Delsate, D., Thies, D., Cuny, G., Pucéat, E., Charbonnier, G., Bayon, G., 2015. Nd isotope constraints on ocean circulation, paleoclimate, and continental drainage during the Jurassic breakup of Pangea. Gondwana Res. 27, 1599–1615.
Dong, T., Harris, N.B., Ayranci, K., 2018. Relative sea-level cycles and organic matter accumulation in shales of the Middle and Upper Devonian Horn River Group, northeastern British Columbia, Canada: insights into sediment flux, redox conditions, and bioproductivity. Geol. Soc. Am. Bull. 130, 859–880.
Dopieralska, J., 2003. Neodymium Isotopic Composition of Conodonts as a Palaeoceanographic Proxy in the Variscan Oceanic System. Justus-Liebig-University, Giessen, pp. 111. http://geb.unigiessen.de/geb/volltexte/2003/1168.
Dopieralska, J., 2009. Reconstructing seawater circulation on the Moroccan shelf of Gondwana during the Late Devonian: evidence from Nd isotope composition of conodonts. Geochem. Geophys. Geosyst. 10, Q03015.
Dopieralska, J., Bełka, Z., Haack, U., 2006. Geochemical decoupling of water masses in the Variscan oceanic system during Late Devonian times. Palaeogeogr. Palaeoclimatol. Palaeoecol. 240, 108–119.
Dopieralska, J., Belka, Z., Königshof, P., Racki, G., Savage, N.M., Lutat, P., Sardsud, A., 2012. Nd isotopic composition of Late Devonian seawater in western Thailand: geotectonic implications for the origin of the Sibumasu terrane. Gondwana Res. 22, 1102–1109.
Dopieralska, J., Belka, Z., Walczak, A., 2016. Nd isotope composition of conodonts: an accurate proxy of sea-level fluctuations. Gondwana Res. 34, 284–295.
Fontaine, H., Hoang, T.T., Juanngam, S., Kavinate, S., Salyapongsse, S., Sutethorn, V., Vachard, D., 2009. Paleontology and Stratigraphy of the Northwest Thailand: Paleogeographical Implications. Department of Mineral Resources, Bangkok, Thailand, pp. 207.
Franchi, F., Turetta, C., Cavalazzi, B., Corami, F., Barbieri, R., 2016. Trace elements and REE geochemistry of Middle Devonian carbonate mounds (Maïder Basin, Eastern Anti-Atlas, Morocco): implications for early diagenetic processes. Sediment. Geol. 343, 56–71.
George, A.D., Chow, N., Trinajstic, K.M., 2014. Oxic facies and the Late Devonian mass extinction, Canning Basin, Australia. Geology 42, 327–330.
Gereke, M., Schindler, E., 2012. "Time-Specific Facies" and biological crises—The Kellwasser Event interval near the Frasnian/Famennian boundary (Late Devonian). Palaeogeogr. Palaeoclimatol. Palaeoecol. 367–368, 19–29.
Gingras, M.K., Pemberton, S.G., Muelenbachs, K., Machel, H., 2004. Conceptual models for burrow-related, selective dolomitization with textural and isotopic evidence from the Tyndall Stone. Canada. Geobiol. 2, 21–30.
Grasby, S.E., Beauchamp, B., Bond, D.P.G., Wignall, P., Talavera, C., Galloway, J.M., Piepjohn, K., Reinhardt, L., Blomeier, D., 2015. Progressive environmental deterioration in northwestern Pangea leading to the latest Permian extinction. Geol. Soc. Am. Bull. 127, 1331–1347.
Grasby, S.E., Them, T.R., Chen, Z., Yin, R.S., Ardakani, O.H., 2019. Mercury as a proxy for volcanic emissions in the geologic record. Earth-Sci. Rev. 196 (102188), 1–16.
Gurvich, E., 2006. Metalliferous Sediments of the World Ocean: Fundamental Theory of Deep-Sea Hydrothermal Sedimentation. Springer, Berlin, pp. 416.
Hagen, D., Kemper, E., 1976. Geology of the Thong Pha Phum area (Kanchanaburi province, western Thailand). Geologisches Jahrbuch B21, 53–91.
Hara, H., Kurihara, T., Kuroda, J., Adachi, Y., Kurita, H., Wakita, K., Hisada, K.-I.,

Charusiri, P., Charoentitirat, T., Chaodumrong, P., 2010. Geological and geochemical aspects of a Devonian siliceous succession in northern Thailand: implications for the opening of the Paleo-Tethys. Palaeogeogr. Palaeoclimatol. Palaeoecol. 207, 452–464.
Harris, N.B., McMillan, J.M., Knapp, L.J., Mastalerz, M., 2018. Organic matter accumulation in the Upper Devonian Duvernay Formation, Western Canada Sedimentary Basin, from sequence stratigraphic analysis and geochemical proxies. Sediment. Geol. 376, 185–203.
Hillbun, K., Playton, T.E., Tohver, E., Ratcliffe, K., Trinajstic, K., Roelofs, B., Caulfield-Kerney, S., Wray, D., Haines, P., Hocking, R., Katz, D., Montgomery, P., Ward, P., 2015. Upper Kellwasser carbon isotope excursion pre-dates the F-F boundary in the Upper Devonian Lennard Shelf carbonate system, Canning Basin, Western Australia. Palaeogeogr. Palaeoclimatol. Palaeoecol. 438, 180–190.
Hladil, J., Krejci, Z., Kalvoda, J., Ginter, M., Galle, A., Beroušek, P., 1991. Carbonate ramp environment of Kellwasser time-interval (Lesni lom, Moravia, Czechoslovakia). Bull. Soc. Belge Géol. 100, 57–119.
Holmden, C., Mitchell, C.E., LaPorte, D.F., Patterson, W.P., Melchin, M.J., Finney, S.C., 2013. Nd isotope records of late Ordovician sea-level change—implications for glaciation frequency and global stratigraphic correlation. Palaeogeogr. Palaeoclimatol. Palaeoecol. 386, 131–144.
Hood, A.S., Planavsky, N.J., Wallace, M.W., Wang, X.G., 2018. The effects of diagenesis on geochemical paleoredox proxies in sedimentary carbonates. Geochim. Cosmochim. Acta 232, 265–287.
Horiike, T., Yamashita, M., 2015. A new fungal isolate, *Penidiella* sp. strain T9, accumulates the rare earth element dysprosium. Appl. Env. Microbiol. 81, 3062–3068.
Huang, C., Joachimski, M.M., Gong, Y.M., 2018a. Did climate changes trigger the Late Devonian Kellwasser Crisis? Evidence from a high-resolution conodont $\delta^{18}O_{PO4}$ record from South China. Earth Planet. Sci. Lett. 495, 174–184.
Huang, C., Song, J.J., Shen, J., Gong, Y.M., 2018b. The influence of the Late Devonian Kellwasser events on deep-water ecosystems: evidence from palaeontological and geochemical records from South China. Palaeogeogr. Palaeoclimatol. Palaeoecol. 504, 60–74.
Hughes, K.P., MacLeod, K.G., Haynes, S.J., Quinton, P.C., Martin, E.E., Ethington, R., 2015. Apaired neodymium and oxygen isotopic perspective on paleoceanographic changes across the Dubuque/Maquoketa contact in the Late Ordovician Laurentian seaway. Stratigraphy 12, 275–285.
Immenhauser, A., Holmden, C., Patterson, W.P., 2008. Interpreting the carbon-isotope record of ancient shallow epeiric seas: lessons from the recent. In: In: Pratt, B., Holmden, C. (Eds.), Dynamics of Epeiric Seas, Geol. Assoc. Canada Spec. Pap. 48. pp. 137–174.
Joachimski, M.M., Buggisch, W., 1993. Anoxic events in the late Frasnian—causes of the Frasnian-Famennian faunal crisis? Geology 21, 675–678.
Joachimski, M.M., Buggisch, W., 2002. Conodont apatite $\delta^{18}O$ signatures indicate climatic cooling as a trigger of the Late Devonian mass extinction. Geology 30, 711–714.
Joachimski, M.M., Ostertag-Henning, C., Pancost, R.D., Strauss, H., Freeman, K.H., Littke, R., DamsteRacki, J.S.S.G., 2001. Water column anoxia, enhanced productivity and concomitant changes in $\delta^{13}C$ and $\delta^{34}S$ across the Frasnian–Famennian boundary (Kowala—Holy Cross Mountains/Poland). Chem. Geol. 175, 109–131.
Joachimski, M.M., Pancost, R.D., Freeman, K.H., Ostertag-Henning, C., Buggisch, W., 2002. Carbon isotope geochemistry of the Frasnian-Famenian transition. Palaeogeogr. Palaeoclimatol. Palaeoecol. 181, 91–109.
Joachimski, M.M., Breisig, S., Buggisch, W., Talent, J.A., Mawson, R., Gereke, M., Morrow, J.R., Day, J., Weddige, K., 2009. Devonian climate and reef evolution: insights from oxygen isotopes in apatite. Earth Planet. Sci. Lett. 284, 599–609.
Johnson, J.G., Klapper, G., Sandberg, C.A., 1985. Devonian eustatic fluctuations in Euramerica. Geol. Soc. Am. Bull. 96, 567–587.
Jones, M.T., Percival, L.M.E., Stokke, E.W., Frieling, J., Mather, T.A., Riber, L., Schubert, B.A., Schultz, S., Tegner, C., Planke, S., Svensen, H.H., 2018. Mercury anomalies across the Palaeocene-Eocene Thermal Maximum. Clim. Past 15, 217–236.
Kamata, Y., Ueno, K., Hara, H., Ichise, M., Charoentitirat, T., Charusiri, P., Sardsud, A., Hisada, K., 2009. Classification of the Sibumasu and Paleo-Tethys tectonic division in Thailand using chert lithofacies. Island Arc 18, 21–31.
Kiipli, E., Kiipli, T., Kallaste, T., Siir, S., 2012. Al_2O_3/TiO_2 ratio of the clay fraction of Late Ordovician-Silurian carbonate rocks as an indicator of paleoclimate of the Fennoscandian Shield. Palaeogeogr. Palaeoclimatol. Palaeoecol. 365–366, 312–320.
Königshof, P., Savage, N.M., Lutat, P., Sardsud, L., Dopieralska, J., Belka, Z., Racki, G., 2012. Late Devonian sedimentary record of the Paleotethys Ocean – The Mae Sariang section, northwestern Thailand. J. Asian Earth Sci. 52, 146–157.
Komatsu, T., Urakawa, R., Inada, T., Yamaguchi, K., Maekawa, T., Takashima, R., Williams, M., Nguyen, D.P., Doan, H.D., Nguyen, M.T., Niko, S., Tanaka, G., Yamaguchi, T., 2019. The Kellwasser events in the Upper Devonian Frasnian to Famennian transition in the Toc Tat Formation, northern Vietnam. Island Arc. 28 (e12281), 1–17.
Königshof, P., Narkiewicz, K., Ta Hoa, P., Carmichael, S., Waters, J., 2017. Events in the mid-Paleozoic: examples from the eastern Paleotethys (Si Phai section, NE Vietnam). Palaeobio. Palaeoenv. 97, 481–496.
Lash, G.G., 2017. A multiproxy analysis of the Frasnian-Famennian transition in western New York State, U.S.A. Palaeogeogr. Palaeoclimatol. Palaeoecol. 473, 108–122.
Lazar, I., Gradinaru, M., Petrescu, L., 2013. Ferruginuous microstromatolites related to Middle Jurassic condensed sequences and hardgrounds (Bucegi Mountains, Southern Carpathians, Romania). Facies 59, 359–390.
Li, F., Yan, J., Burne, R.V., Chen, Z.Q., Algeo, T.J., Zhang, W., Tian, L., Gan, Y., Liu, K., Xie, S., 2017. Paleo-seawater REE compositions and microbial signatures preserved in laminae of Lower Triassic ooids. Palaeogeogr. Palaeoclimatol. Palaeoecol. 486, 96–107.
Lo, F.L., Chen, H.F., Fang, J.N., 2017. Discussion of suitable chemical weathering proxies in sediments by comparing the dissolution rates of minerals in different rocks. J. Geol. 125, 83–99.
Loydell, D.K., 2007. Early Silurian positive $\delta^1$3C excursions and their relationship to glaciations, sea-level changes, and extinction events. Geol. J. 42, 531–546.
Ma, X., Gong, Y., Chen, D., Racki, G., Chen, X., Liao, W., 2016. The Late Devonian Frasnian-Famennian Event in South China—Patterns and causes of extinctions, sea level changes, and isotope variations Palaeogeogr. Palaeoclimatol. Palaeoecol. 448, 224–244.
McLennan, S.M., 2001. Relationships between the trace element composition of sedimentary rocks and upper continental crust. Geochem. Geophys. Geosyst. 2 2000GC000I09.
McLennan, S.M., Hemming, S., Mcdaniel, D.K., Hanson, G.N., 1993. Geochemical approaches to sedimentation, provenance and tectonics. In: In: Johansson, M.J., Basu, A. (Eds.), Processes Controlling the Composition of Clastic Sediments. Geol. Soc. Am. Spec. Pap. 284. pp. 21–40.
McGhee, G.R., 2013. When the Invasion of Land Failed: The Legacy of the Devonian Extinctions. Columbia University Press, New York, pp. 336.
Metcalfe, I., 1984. Stratigraphy, palaeontology and palaeogeography of the Carboniferous of Southeast Asia. Mem. Soc. Geol. France 147, 107–118.
Metcalfe, I., 1996. Gondwanaland dispersion, Asian accretion and evolution of Eastern. Tethys. Austral. J. Earth Sci. 43, 605–623.
Metcalfe, I., 1999. Gondwana dispersion and Asian accretion, an overview. In: Metcalfe, I. (Ed.), Gondwana Dispersion and Asian Accretion (IGCP 321 Final Results Volume). A.A. Balkema, Rotterdam, pp. 1–33.
Metcalfe, I., 2006. Palaeozoic and Mesozoic tectonic evolution and palaeogeography of East Asian crustal fragments: the Korean Peninsula in context. Gondwana Res. 9, 24–46.
Metcalfe, I., 2009. Comment on An alternative plate tectonic model for the Palaeozoic-Early Mesozoic Palaeotethyan evolution of Southeast Asia (Northern Thailand-Burma). Tectonophysics 451, 346–365.
Metcalfe, I., 2011. Tectonic framework and Phanerozoic evolution of Sundaland. Gondwana Res. 19, 3–21.
Metcalfe, I., 2013. Gondwana dispersion and Asian accretion: tectonic and palaeogeographic evolution of eastern Tethys. J. Asian Earth Sci. 66, 1–33.
Morley, C.K., Charusiri, P., Watkinson, I.M., 2011. Structural Geology of Thailand during the Cenozoic. In: Ridd, M.F., Barber, A.J., Crow, M.J. (Eds.), The Geology of Thailand. Geological Society, London, pp. 273–334.
Morrow, J.R., Sandberg, C.A., 2008. Evolution of Devonian carbonate-shelf margin, Nevada. Geosphere 4, 445–458.
Murray, R.W., 1994. Chemical criteria to identify the depositional environment of chert: general principles and applications. Sed. Geol. 90, 213–232.
Nath, B., Jean, J.S., Lee, M.K., Yang, H.J., Liu, C.C., 2008. Geochemistry of high arsenic groundwater in Chia-Nan plain, Southwestern Taiwan: possible sources and reactive transport of arsenic. J. Contam. Hydrol. 99, 85–96.
Nie, S., Rowley, D.B., Ziegler, A.M., 1990. Econstrains on the locations of Asian microcontinents in Paleo-Tethys during the Late Paleozoic. In: In: McKerrow, W.S., Scotese, C.R. (Eds.), Palaeozoic Palaeogeography and Biogeography, Geol. Soc, London Spec. Mem. 12. pp. 397–409.
Nothdurft, L.D., Webb, G.E., Kamber, B.S., 2004. Rare earth element geochemistry of Late Devonian reefal carbonates, Canning Basin, Western Australia: confirmation of a seawater REE proxy in ancient limestones. Geochim. Cosmochim. Acta 68, 263–283.
Ocubalidet, S.G., Rimmer, S.M., Conder, J.A., 2018. Redox conditions associated with organic carbon accumulation in the Late Devonian New Albany Shale, west-central Kentucky. Illinois Basin. Intern. J. Coal Geol. 190, 42–55.
Over, D.J., 2002. The Frasnian/Famennian boundary in central and eastern United States. Palaeogeogr. Palaeoclimatol. Palaeoecol. 181, 153–169.
Panchuk, K.M., Holmden, C.E., Leslie, S.S., 2006. Local controls on carbon cycling in the Ordovician Midcontinent region of North America with implications for carbon isotope secular curves. J. Sediment. Res. 76, 200–211.
Percival, L.M.E., Jenkyns, H.C., Mather, T.A., Dickson, A.J., Batenburg, S.J., Ruhl, M., Hesselbo, S.P., Barclay, R., Jarvis, J., Robinson, S.A., Woelders, L., 2018. Does Large Igneous Province volcanism always perturb the mercury cycle? Comparing the records of Oceanic Anoxic Event 2 and the end-Cretaceous to other Mesozoic events. Am. J. Sci. 318, 799–860.
Percival, L.M.E., Selby, D., Bond, D.P.G., Rakociński, M., Racki, G., Marynowski, L., Adatte, T., Spangenberg, J.E., Föllmi, K.B., 2019. Pulses of enhanced continental weathering associated with multiple Late Devonian climate perturbations: evidence from osmium- isotope compositions. Palaeogeogr. Palaeoclimatol. Palaeoecol 524, 240–249.
Pisarzowska, A., Racki, G., 2012. Isotopic chemostratigraphy across the Early-Middle Frasnian transition (Late Devonian) on the South Polish carbonate shelf: a reference for the global punctata Event. Chem. Geol. 334, 199–220.
Pujol, F., Berner, Z., Stüben, D., 2006. Palaeoenvironmental changes at the Frasnian/Famennian boundary in key European sections: chemostratigraphic constraints. Palaeogeogr. Palaeoclimatol. Palaeoecol. 240, 120–145.
Preat, A., Mamet, B., De Ridder, C., Boulvain, F., Gillan, D., 2000. Iron bacterial and fungal mats, Bajocian stratotype (Mid-Jurassic, northern Normandy, France). Sediment. Geol. 137, 107–126.
Racka, M., Marynowski, L., Filipiak, P., Sobstel, M., Pisarzowska, A., Bond, D.P.J., 2010. Anoxic Annulata events in the Late Famennian of the Holy Cross Mountains (Southern Poland): geochemical and palaeontological record. Palaeogeogr. Palaeoclimatol. Palaeoecol. 297, 549–575.
Racki, G., 1998. Frasnian-Famennian biotic crisis: undervalued tectonic control? Palaeogeogr. Palaeoclimatol. Palaeoecol. 141, 77–198.
Racki, G., 1999. Silica-secreting biota and mass extinctions: survival patterns and processes. Palaeogeogr. Palaeoclimatol. Palaeoecol. 154, 107–132.
Racki, G., 2005. Towards understanding Late Devonian global events: few answers, many questions. In: In: Over, D.J., Morrow, J.R., Wignall, P.B. (Eds.), Understanding Late Devonian and Permian–Triassic Biotic and Climatic Events: Towards an Integrated Approach. Developments in Palaeontology & Stratigraphy 20. Elsevier, Amsterdam, pp. 5–36.
Racki, G., Racka, M., Matyja, H., Devleeschouwer, X., 2002. The Frasnian/Famennian boundary interval in the South Polish-Moravian shelf basins: integrated event-tratigraphical approach. Palaeogeogr. Palaeoclimatol. Palaeoecol. 181, 251–297.

Racki, G., Baliński, A., Wrona, R., Małkowski, K., Drygant, D., Szaniawski, H., 2012. Faunal dynamics across the Silurian-Devonian positive isotope excursions ($\delta^{13}C$, $\delta^{18}O$) in Podolia, Ukraine: comparative analysis of the Ireviken and Klonk events. Acta Palaeontol. Pol. 57, 795–832.
Racki, G., Marynowski, L., Rakociński, M., 2018a. Anomalous Upper Devonian mercury enrichments - comparison of Inductively Coupled Plasma-Mass Spectrometry (ICP-MS) and Atomic Absorption Spectrometry (AAS) analytical data. Geol. Quart. 62, 487–495.
Racki, G., Rakociński, M., Marynowski, L., Wignall, P.B., 2018b. Mercury enrichments and the Frasnian-Famennian biotic crisis: a volcanic trigger proved? Geology 46, 543–546.
Ramkumar, M. (Ed.), 2016. Chemostratigraphy: Concepts, Techniques and Applications. Elsevier, Amsterdam, pp. 538.
Randon, C., Wonganan, N., Caridroit, M., Perret, M.M.F., Degardin, J.M., 2006. Upper Devonian-Lower Carboniferous conodonts from Chiang Dao cherts, northern Thailand. Riv. Ital. Palaeont. Strat. 112, 191–206.
Ratcliffe, K.T., Wright, A.M., Montgomery, P., Palfrey, A., Vonk, A., Vermeulen, J., Barrett, M., 2010. Application of chemostratigraphy to the Mungaroo Formation, the Gorgon Field, offshore Northwest Australia. APPEA Journal 50th Anniversary Issue 371–388.
Reolid, M., Abad, I., Martın-Garcıa, J.M., 2008. Palaeoenvironmental implications of ferruginous deposits related to a Middle-Upper Jurassic discontinuity (Prebetic Zone, Betic Cordillera, Southern Spain). Sediment. Geol. 203, 1–16.
Reolid, M., Nieto, L.M., 2010. Jurassic Fe–Mn macro-oncoids from pelagic swells of the external subbetic (Spain): evidences of microbial origin. Geol. Acta 8, 151–168.
Retallack, G.J., Huang, C.M., 2011. Ecology and evolution of Devonian trees in New York, USA. Palaeogeogr. Palaeoclimatol. Palaeoecol. 299, 110–128.
Riboulleau, A., Spina, A., Vecoli, M., Riquier, L., Quijada, M., Tribovillard, N., Averbuch, O., 2018. Organic matter deposition in the Ghadames Basin (Libya) during the Late Devonian: a multidisciplinary approach. Palaeogeogr. Palaeoclimatol. Palaeoecol. 497, 37–51.
Ridd, M.F., 2009. The Phuket Terrane: a Late Palaeozoic rift at the margin of Sibumasu. J. Asian Earth Sci. 36, 238–251.
Ridd, M.F., 2011. Lower Palaeozoic. In: Ridd, M.F., Barber, A.J., Crow, M.J. (Eds.), The Geology of Thailand. Geological Society, London, pp. 33–51.
Ridd, M.F., 2012. The role of strike-slip faults in the displacement of the Palaeotethys suture zone in Southeast Thailand. J. Asian Earth Sci. 51, 63–84.
Ridd, M.F., 2015. East flank of Sibumasu block in NW Thailand and Myanmar and its possible northward continuation into Yunnan: a review and suggested tectono-stratigraphic interpretation. J. Asian Earth Sci. 104, 160–174.
Riquier, L., Tribovillard, N., Averbuch, O., Devleeschouwer, X., Riboulleau, A., 2006. The Late Frasnian Kellwasser horizons of the Harz Mountains (Germany): two oxygen-deficient periods resulting from different mechanisms. Chem. Geol. 233, 137–155.
Rosenbaum, G., 2018. The Tasmanides: Phanerozoic tectonic evolution of Eastern Australia. Annu. Rev. Earth Planet. Sci. 46, 291–325.
Sageman, B.B., Lyons, T.W., 2003. Geochemistry of fine-grained sediments and sedimentary rocks. Treatise Geochem. 7, 115–158.
Sageman, B.B., Murphy, A.E., Werne, J.P., Ver Straeten, C.A., Hollander, D.J., Lyons, T.W., 2003. A tale of shales: the relative roles of production, decomposition, and dilution in the accumulation of organic-rich strata, Middle-Upper Devonian, Appalachian basin. Chem. Geol. 195, 229–273.
Sandberg, C.A., Ziegler, W., Dreesen, R., Butler, J., 1988. Late Frasnian mass extinction: conodont event stratigraphy, global changes, and possible causes. Cour. Forsch. Senckenberg 102, 263–307.
Savage, N.M., 2013. Late Devonian Conodonts from Northwestern Thailand. Bourland Printing/Trinity Press, Eugene, Oregon, pp. 48.
Savage, N.M., 2019. Frasnian-Famennian transition in western Thailand: conodonts, biofacies, eustatic changes, extinction. J. Paleont. 93, 476–495.
Savage, N.M., Sardsud, A., Buggisch, W., 2006. Late Devonian conodonts and the global Frasnian-Famennian extinction event, Thong Pha Phum, western Thailand. Paleoworld 15, 171–184.
Śliwiński, M.G., Whalen, M.T., Meyer, F.J., Majs, F., 2012. Constraining clastic input controls on magnetic susceptibility and trace element anomalies during the Late Devonian punctata Event in the Western Canada Sedimentary Basin. Terra Nova 24, 301–309.
Sone, M., Metcalfe, I., 2008. Parallel Tethyan sutures in mainland SE Asia: new insights for Palaeo-Tethys closure. C. R. Geosci. 340, 166–179.
Song, H.J., Algeo, T.J., Tong, J.N., Romaniello, S.J., Zhu, Y.Y., Chu, D.L., Anbar, A.D., 2017. Uranium and carbon isotopes document global-ocean redox-productivity relationships linked to cooling during the Frasnian-Famennian mass extinction. Geology 45, 887–890.
Spalletta, C., Perri, M.C., Over, D.J., Corradini, C., 2017. Famennian (Upper Devonian) conodont zonation: revised global standard. Bull. Geosci. 92, 31–57.
Stanley, S.M., 2016. Estimates of the magnitudes of major marine mass extinctions in Earth history. Proc. Natl. Acad. Sci. U. S. A. 113, 6325–6334.
Stephens, N.P., Sumner, D.Y., 2003. Late Devonian carbon isotope stratigraphy and sea level fluctuations, Canning Basin, Western Australia. Palaeogeogr. Palaeoclimatol. Palaeoecol. 191, 203–219.
Suzuki, N., Ishida, K., Shinomiya, Y., Ishiga, H., 1998. High productivity in the earliest Triassic ocean: Black shales, Southwest Japan. Palaeogeogr. Palaeoclimatol. Palaeoecol. 141, 53–65.
Swart, P.K., 2015. The geochemistry of carbonate diagenesis: the past, present and future. Sedimentology 62, 1233–1304.
Sweere, T., Sander van den, B., Dickson, A.J., Reichart, G.J., 2016. Definition of new trace-metal proxies for the controls on organic matter enrichment in marine sediments based on Mn Co, Mo and Cd concentrations. Chem. Geol. 441, 235–245.
Takahashi, Y., Châtellier, X., Hattori, K.H., Kato, K., Fortin, D., 2005. Adsorption of rare earth elements onto bacterial cell walls and its implication for REE sorption onto natural microbial mats. Chem. Geol. 219, 53–67.
Taylor, S.R., McLennan, S.M., 1985. The Continental Crust: Its Composition and Evolution. Blackwell, Oxford, pp. 312.
Thassanapak, H., Udchachon, M., Burrett, C., Feng, Q., 2017. Geochemistry of radiolarian cherts from a Late Devonian continental margin, Loei Foldbelt, Indochina terrane. J. Earth Sci. 28 (1), 9–28.
Torsvik, T.H., Cocks, R.M., 2017. Earth History and Palaeogeography. Cambridge University Press, Cambridge, pp. 317.
Tribovillard, N., Algeo, T.J., Lyons, T., Riboulleau, A., 2006. Trace metals as paleoredox and paleoproductivity proxies: an update. Chem. Geol. 232, 12–32.
Tulipani, S., Grice, K., Greenwood, P.F., Haines, P.W., Sauer, P.E., Schimmelmann, A., Summons, R.E., Foster, C.B., Böttcher, M.E., Playton, T., Schwark, L., 2015. Changes of palaeoenvironment conditions recorded in Late Devonian reef systems from the Canning Basin, Western Australia: a biomarker and stable isotope approach. Gondwana Res. 28, 1500–1515.
Udchachon, M., Thassanapak, H.M., Burrett, C., 2017a. Palaeoenvironment and palaeogeography of Middle and Upper Devonian strata from the Loei fold belt, Indochina terrane (northeast Thailand). Palaeobio. Palaeoenv. 97, 497–516.
Udchachon, M., Thassanapak, H.M., Feng, Q., Burrett, C., 2017b. Palaeoenvironmental implications of geochemistry and radiolarians from Upper Devonian chert/shale sequences of the Truong Son fold belt. Laos. Geol. J. 52, 154–173.
Ueno, K., Charoentitirat, T., 2011. Carboniferous and Permian. In: Ridd, M.F., Barber, A.J., Crow, M.J. (Eds.), The Geology of Thailand. Geological Society, London, pp. 71–136.
Ueno, K., Miyahigashi, A., Charoentitirat, T., 2010. The Lopingian (Late Permian) of mid-oceanic carbonates in the Eastern Palaeotethys: stratigraphical outline and foraminiferal faunal succession. Geol. J. 45, 285–307.
Van der Weijden, C.H., 2002. Pitfalls of normalization of marine geochemical data using a common divisor. Mar. Geol. 184, 167–187.
Ver Straeten, C.A., Brett, C.E., Sageman, B.B., 2011. Mudrock sequence stratigraphy: a multi−proxy (sedimentological, paleobiological and geochemical) approach, Devonian Appalachian Basin. Palaeogeogr. Palaeoclimatol. Palaeoecol. 304, 54–73.
Walliser, O.H., 1984. Pleading for a natural D/C-boundary. Cour. Forsch. Senckenberg 67, 241–246.
Walliser, O.H., 1996. Global events in the Devonian and Carboniferous. In: Walliser, O.H. (Ed.), Global Events and Event Stratigraphy. Springer, Berlin, Heidelberg, New York, pp. 225–250.
Wang, Y.J., Qian, X., Cawood, P.A., Liu, H.C., Feng, Q.L., Zhao, G.C., Zhang, Y.H., He, H.Y., Zhang, P.Z., 2018. Closure of the East Paleotethyan Ocean and amalgamation of the Eastern Cimmerian and Southeast Asia continental fragments. Earth-Sci. Rev. 186, 195–230.
Webb, G.E., Kamber, B.S., 2000. Rare earth elements in Holocene reefal microbialites: a new shallow seawater proxy. Geochim. Cosmochim. Acta 64, 1557–1565.
Wedepohl, K.H., 1970. Geochemische Daten von sedimentären Karbonaten und Karbonatgesteinen in ihrem faziellen und petrogenetischen Aussagewert. Verh. Geol. Bundesanstalt 4, 692–705.
Wedepohl, K.H., 1971. Environmental influences on the chemical composition of shales and clays. In: Ahrens, L.H., Press, F., Runcorn, S.K., Urey, H.C. (Eds.), Physics and Chemistry of the Earth. Pergamon Press, Oxford, pp. 307–331.
Wedepohl, K.H., 1991. The composition of the upper earth's crust and the natural cycles of selected metals. Metals in natural raw materials. Natural Resources. In: Merian, E. (Ed.), Metals and Their Compounds in the Environment. Verlag Chemie (VCH), Weinheim, pp. 3–17.
Weiner, T., Kalvoda, J., Kumpan, T., Schindler, E., Šimíček, D., 2017. An integrated stratigraphy of the Frasnian-Famennian boundary interval (Late Devonian) in the Moravian Karst (Czech Republic) and Kellerwald (Germany). Bull. Geosci. 92, 257–281.
Whalen, M., 2015. Chemostratigraphy and magnetic susceptibility of the Late Devonian Frasnian–Famennian transition in western Canada and southern China: implications for carbon and nutrient cycling and mass extinction. In: In: Da Silva, A.C., Whalen, M.T., Hladil, J., Chadimova, L., Chen, D., Spassov, S., Boulvain, F., Devleeschouwer, X. (Eds.), Magnetic Susceptibility Application: A Window onto Ancient Environments and Climatic Variations. Geol. Soc, London Spec. Publ. 414. pp. 37–72.
Whalen, M., De Vleeschouwer, D., Payne, J., Day, J., Over, J., Claeys, P., 2017. Pattern and timing of the Late Devonian biotic crisis in Western Canada: insights from carbon isotopes and astronomical calibration of magnetic susceptibility data. In: New Advances in Devonian Carbonates: Outcrop Analogs, Reservoirs, and Chronostratigraphy, SEPM Spec. Publ. 107. pp. 185–201.
Winter, J., 2015. Vulkanismus und Kellwasser-Krise – Zirkon-Tephrostratigrafie, Identifizierung und Herkunft distaler Fallout-Aschenlagen (Oberdevon, Synklinorium von Dinant, Rheinisches Schiefergebirge, Harz). Z. Dtsch. Gesell. Geowiss. 166, 227–251.
Wonganan, N., Caridroit, M., 2005. Middle and Upper radiolarian faunas from Chiang Dao area. Chiang Mai Province, northern Thailand. Micropaleontology 51, 39–57.
Wonganan, N., Randon, C., Caridroit, M., 2007. Mississippian (early Crboniferous) radiolarian biostratigraphy of northern Thailand (Chian Dao area). Geobios 40, 875–888.
Xu, B., Gu, Z., Wang, C., Hao, Q., Han, J., Liu, Q., Wang, L., Lu, Y., 2012. Carbon isotopic evidence for the associations of decreasing atmospheric CO2 level with the Frasnian-Famennian mass extinction. J. Geophys. Res. Biogeosci. 117, 1–12.
Yudina, A.B., Racki, G., Savage, N.S., Racka, M., Małkowski, K., 2002. The Frasnian-Famennian events in a deep-shelf succession, Subpolar Urals: biotic, depositional and geochemical records. Acta Palaeont. Pol. 47, 355–372.
Zatoń, M., Kremer, B., Marynowski, L., Wilson, M.A., Krawczyński, W., 2012. Middle Jurassic (Bathonian) encrusted oncoids from the Polish Jura, southern Poland. Facies 58, 57–77.
Zhang, K.J., Li, Q.-H., Yan, L.-L., Zeng, L., Lu, L., Zhang, Y.-X., Hui, J., Jin, X., Tang, X.-C., 2017. Geochemistry of limestones deposited in various plate tectonic settings. Earth-Sci. Rev. 167, 27–46.
Zhang, X.C., Wang, Y.J., Harris, R., Yan, Y., Zheng, Y., 2019. Discovery of Middle-Late Devonian and Early Permian magmatic events in East Asia and their implication for the Indosinian orogeny in South China: insights from the sedimentary record. Geol. Soc. Am. Bull. 131, 1519–1536. https://doi.org/10.1130/B35032.1.